https://doi.org/10.5194/egusphere-2026-103
Preprint. Discussion started: 29 January 2026

Quantitative assessment of parameterization sensitivity and uncertainty in Noah-MP multi-physics ensemble simulations of gross primary productivity across China's terrestrial ecosystem

Jie Lai[a,b], Anzhi Wang[a], Yage Liu[a], Lidu Shen[a], Yuan Zhang[a], Yiwei Diao[c], Rongrong Cai[a], Rongping Li[d], Wenli Fei[a,*], Jiabing Wu[a,*]

[a] CAS Key Laboratory of Forest Ecology and Silviculture, Institute of Applied Ecology, Chinese Academy of Sciences, Shenyang, China
[b] University of Chinese Academy of Sciences, Beijing, China
[c] Key Laboratory of Ecosystem Carbon Source and Sink, China Meteorological Administration, Wuxi University, Wuxi, China
[d] Institute of Atmospheric Environment, China Meteorological Administration, Shenyang, China

* Corresponding author
E-mail: Wenli Fei（feiwenli@iae.ac.cn) and Jiabing Wu (wujb@iae.ac.cn)

Abstract

Understanding the carbon cycle and its interactions with climate systems requires precise simulation of Gross Primary Productivity (GPP). However, achieving this remains challenging due to the inherent complexity of the models. Current research lacks quantification of how uncertainties in physical process parameterization affect GPP simulation across various ecosystems, and the dominant physical processes goberning GPP variability are pooly identified. To address these issues, this study generated a 48-member Noah Land Surface Model with multi-parameterization options (Noah-MP) ensemble by manipulating key physical parameterization schemes. The model was validated using ChinaFlux tower measurements and Penman-Monteith–Leuning Version 2 data. We employed the Sobol' total sensitivity index to assess the influence of four key physical processes on GPP: radiation transfer, the soil moisture limitation factor for transpiration (β-factor), turbulence, and runoff generation. Results demonstrate that Noah-MP effectively captured GPP's spatiotemporal patterns in Chinese ecosystems but overestimated GPP in forest and cropland during spring and summer. Sensitivity analysis indicates that the β-factor dominates GPP simulations across most of China, while radiation transfer is the primary

https://doi.org/10.5194/egusphere-2026-103
Preprint. Discussion started: 29 January 2026

driver on the Tibetan Plateau. The main difference between the two radiation transfer schemes lies in whether vegetation gaps fraction are considered. On the Tibetan Plateau, where grasslands and shrublands exhibit large canopy gaps, consider it or not could lead to in substantial differences in simulated radiation and consequently in GPP, making GPP highly sensitive to the choice of radiation scheme. Across ecosystems, water-related factors (β-factor and runoff) mainly affect croplands and savannas, radiation transfer dominates grasslands and shrublands, and turbulence is most influential in forests. There are also distinct seasonal patterns: radiation and turbulence dominate in spring and summer, while radiation and β-factor prevail in autumn and winter, especially in arid regions. Based on systematic performance evaluations and sensitivity analyses, this study proposes optimized Noah-MP model configurations for China's terrestrial ecosystems. The radiation transfer scheme considering the three-dimensional canopy structure (option 1) is recommended for grasslands and shrublands. Our findings offer insights for enhancing GPP simulation accuracy in Noah-MP, thereby improving the model's ability to represent carbon–water dynamics from regional to continental scales.

Keywords: Gross Primary Productivity; Noah-MP; Uncertainty; Parameterization sensitivity; China

https://doi.org/10.5194/egusphere-2026-103
Preprint. Discussion started: 29 January 2026

1 Introduction

Gross primary productivity (GPP) is an important indicator representing the total carbon assimilated by plants through photosynthesis (Qian et al., 2024; Wang et al., 2023). Precise estimation of GPP is crucial for examining ecosystem carbon cycles and evaluating ecosystem responses to global environmental changes (Chang et al., 2023; H. Wang et al., 2023; Zhang and Ye, 2022). The eddy covariance technique, often regarded as the most reliable approach for quantifying CO_2 fluxes between ecosystems and the atmosphere, is nonetheless limited in spatial coverage, being applicable primarily at local scales (Chen et al., 2020; Yu et al., 2016). Land surface models (LSMs) provide a powerful framework for enabling continuous simulation of GPP at regional scales, thereby advancing understanding of carbon cycle processes and their feedbacks with the climate system (Wei et al., 2017; Sims et al., 2008; Running et al., 2004).

During the last few decades, LSMs have undergone significant advancements through three major stages, each aimed at improving the realism of physical parameterization and achieving higher accuracy in simulating carbon, water, and energy cycles (Pitman, 2003; Sellers et al., 1997). First-generation LSMs conceptualize the land surface as a simple bucket with a constant water-holding capacity, significantly oversimplifying soil moisture dynamics and vegetation effects (Manabe, 1969). This simplification leads to unrealistic simulations of energy partitioning and water transferring. Second-generation LSMs are built on the Soil-Vegetation-Atmosphere-Transfer Model, explicitly incorporating interactions and feedback mechanisms among vegetation, atmosphere, and soil (Deardorff, 1977). These models provide a more realistic depiction of land surface processes by integrating stomatal conductance, which regulates transpiration, along with soil layer water exchange. Third-generation LSMs evolve from the second-generation LSMs by incorporating biochemical processes. They recognize vegetation's critical role in terrestrial carbon-water cycles, including its contribution to land evapotranspiration (Jasechko et al., 2013), its modulation of heat and water vapor exchanges to influence precipitation (Green et al., 2017), and its absorption of carbon dioxide via photosynthesis (Vicca, 2018). Currently, the typical third-generation LSMs, such as the Simple Biosphere Model (Denning et al., 1996), the Community Land Model (CLM, Oleson et al., 2010), and the Noah Model with Multiple Parameterizations (Noah-MP, Niu et al., 2011; Yang et al., 2011), have become mainstream tools for land surface research. Take Noah-MP as an example, it introduces a dynamic vegetation module to simulate canopy density and plant coverage across

https://doi.org/10.5194/egusphere-2026-103
Preprint. Discussion started: 29 January 2026

different vegetation types while accounting for carbon allocation within plants (Yang and Niu, 2003; Dickinson et al., 1998). The model incorporates stomatal-photosynthesis coupling for sunlit and shaded leaves, with distinct parameterizations for photosynthesis and respiration in C3 versus C4 plants (Ball et al., 1987; Bonan, 1996). The canopy gaps are considered to compute the absorption of solar radiation by sunlit and shaded leaves (Niu and Yang, 2004; Yang and Friedl, 2003). Third-generation LSMs improve simulation accuracy and allow for the coupling of terrestrial-atmospheric carbon and nitrogen cycles with energy and water fluxes by comprehensively modeling processes such as canopy radiation transfer, soil heat and water transport, and biochemical activity (Pitman, 2003; Dickinson et al., 1998). These advancements have significantly propelled multi-scale studies of climate, ecosystems, and land-atmosphere interactions, thereby improving comprehension of land surface dynamics and their impacts on regional climate variability (He et al., 2024; Yang et al., 2021; Zhang et al., 2016; W. Cai et al., 2014; Baker et al., 2003).

Notwithstanding their broad application, these models continue to suffer from persistent issues that affect the reliability of GPP estimates over China (Wang et al., 2024; Li et al., 2022). For example, Zheng et al. (2023) found that CLM4.5 underestimated GPP in some temperate forests and C3 grasslands, while overestimating GPP in temperate broadleaf evergreen forests. This bias is linked to the model's tendency to overestimate specific leaf area, particularly at the canopy top and on sloped terrain. Similarly, Zhang et al. (2016) reported that while CLM4.5 improved GPP simulation compared to CLM4.0, particularly in subtropical forests, it still exhibited a positive bias in annual GPP. These findings highlight the necessity for improving parameterizations of structural, physiological, and growth-status parameters under different vegetation types. Additionally, Li et al. (2022) noted that Noah-MP shows uncertainty in simulating GPP over China, with relative biases exceeding 40% in grasslands and reaching 100% in drylands, while it performs better in humid areas. The above results indicate that further uncertainty assessments are essential across China's diverse ecosystems. This will facilitate the identification of uncertainty sources and the optimization of parameterization schemes.

Among the above-mentioned LSMs, Noah-MP is particularly suited for uncertainty attribution because it offers multiple parameterization schemes for key physical processes (Clark et al., 2011). Parameterizations for a single physical process often rely on conflicting assumptions. This divergence, rooted in incomplete process knowledge, is a major source of uncertainty in multi-physics ensemble modeling (Clark et al., 2015). By systematically comparing these schemes, researchers can identify optimal configurations tailored to specific climatic and surface conditions, thereby enhancing model adaptability and reliability across diverse environmental scenarios (Chang et al., 2020; Clark et al., 2016). Moreover, Noah-MP can generate ensembles by perturbing specific physical process parameterizations, and enable the quantification of the relative contributions of different parameterizations to total uncertainties through sensitivity analyses. For instance, Zheng et al. (2019) utilized a 48-member Noah-MP multi-physics ensemble with the Sobol' variance decomposition method (Saltelli et al., 2010; Sobol′, 2001; Saltelli and Sobol, 1995) to assess the sensitivity of precipitation partitioning to the parameterizations of relevant physical processes. Yang et al. (2011) and You et al. (2024) employed the Noah-MP multi-physics ensemble to investigate various physical processes' contributions to soil moisture, ET, runoff, and snow depth. For carbon cycle simulations, Yang et al. (2021) employed Noah-MP to analyze the sensitivity of net ecosystem exchange (NEE) at the site scale, highlighting the soil moisture factor for stomatal resistance and surface layer turbulence as the most sensitive processes. Some studies (You et al., 2020; Li et al., 2019) also demonstrated that the primary source of uncertainty in multi-parameter ensemble simulations is attributed to sensitive parameterization schemes. Thus, sensitivity analyses on the Noah-MP multi-physics ensemble can facilitate the selection of effective parameterization scheme combinations, which is vital for enhancing GPP estimation accuracy in diverse ecosystems. Furthermore, quantitative analysis of the impacts of different physical processes on GPP can identify the key factors and driving mechanisms affecting carbon absorption across various ecosystems.

However, existing uncertainty attribution studies based on the Noah-MP multi-physics ensemble have largely focused on hydrological processes at global and regional scales (Zheng et al., 2023; Li et al., 2022), while analyses specific to terrestrial carbon cycle processes remain limited, especially in China. Yang et al. (2021)investigated the key physical processes affecting GPP at the site scale, but their study was constrained to a relatively short period (less than 10 years) and limited sites (eight sites). To date, there is a lack of comprehensive uncertainty attribution studies on GPP simulations over China that account for different vegetation types and both multi-year and seasonal scales. The contributions of different physical processes to GPP simulation uncertainty across China have not been quantitatively determined. The dominant

https://doi.org/10.5194/egusphere-2026-103
Preprint. Discussion started: 29 January 2026

processes affecting GPP across different vegetation types remain unknown. This limitation restricts the improvement of Noah-MP, hindering its practical application in carbon sink assessments and policy-making in China.

To better understand model uncertainties, this study applied the Sobol' sensitivity analysis on a 48-member Noah-MP ensemble across different vegetation types in China over a 20-year period (2001–2020). First, we evaluated the ensemble's uncertainty in simulating GPP over China at seasonal and multi-year mean scales against China Flux sites data and the Penman-Monteith-Leuning Version 2 (PML-V2) GPP dataset, to assess the accuracy and applicability of Noah-MP over China. Subsequently, we quantified and compared the sensitivity of four key physical processes—radiation transfer, soil moisture limitation factor to transpiration (β-factor), surface turbulent exchange (turbulence), and runoff in simulating GPP across China's diverse ecosystems. This study focuses on two main scientific questions: (1) the performance of the Noah-MP ensemble in simulating GPP for different vegetation types in China over seasonal and multi-year periods, and (2) the identification of key physical processes and mechanisms that govern GPP in diverse ecosystems. The study clarifies the influence of physical process parameterizations on GPP simulation within Noah-MP and provides ecosystem-specific recommendations for model configuration, offering valuable insights to enhance the accuracy of terrestrial carbon flux modeling in China. The flowchart of this study is shown in **Figure 1.**

The paper is structured as follows. Section 2 provides a description of the model and datasets, while Section 3 outlines the methods for model evaluation and sensitivity analysis. The results are presented in Section 4, followed by conclusions and discussion in Section 5.

https://doi.org/10.5194/egusphere-2026-103
Preprint. Discussion started: 29 January 2026

165 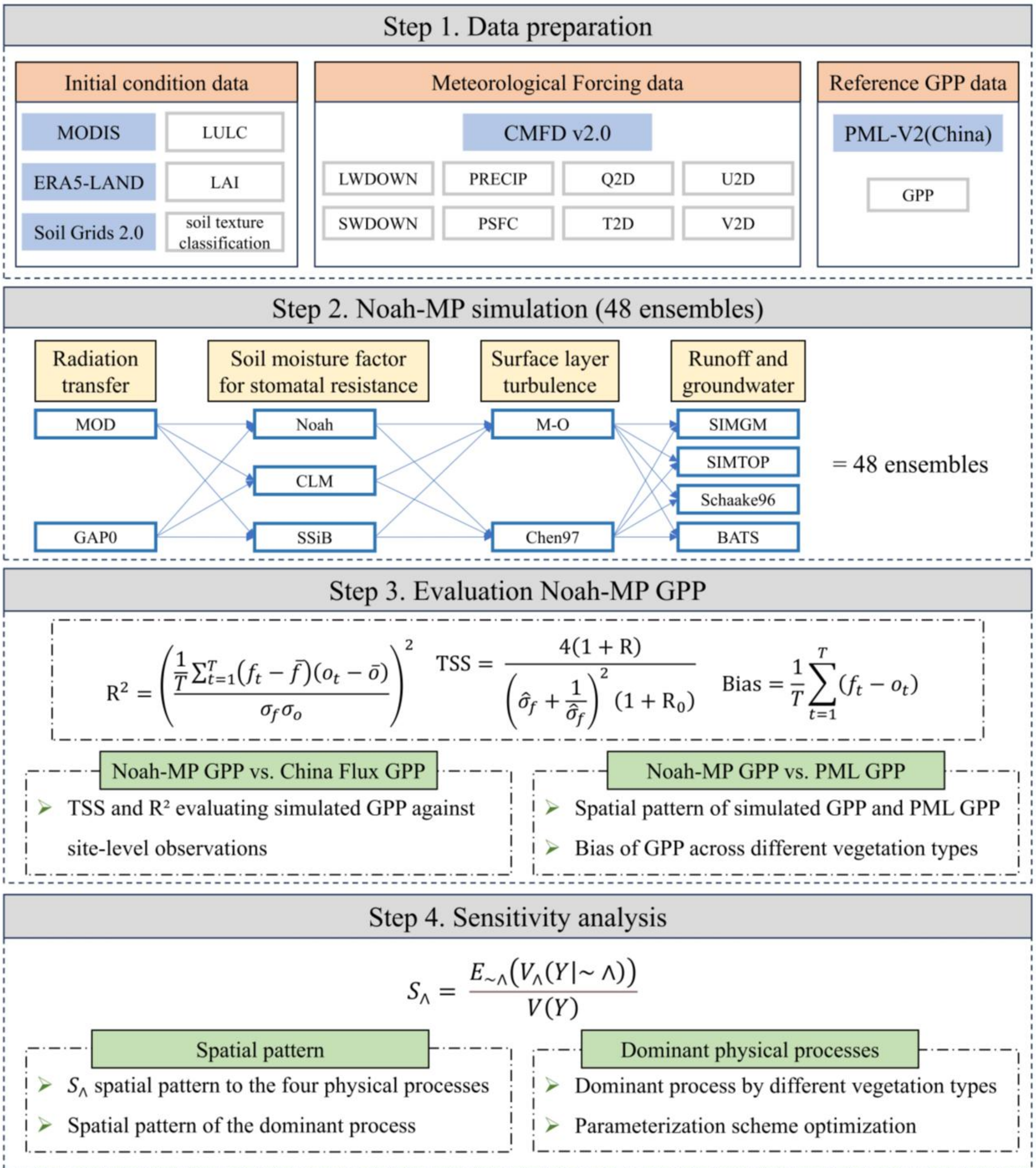

166 **Figure 1**. Flowchart of this study.

https://doi.org/10.5194/egusphere-2026-103
Preprint. Discussion started: 29 January 2026

2 Model and datasets

2.1 Study domain

This study selected China (18.5°N–53.75°N, 73.25°E–135.25°E) as the study domain, as shown in **Figure 1**. China covers a land area of about 9.6 million square kilometers, extending across much of East Asia along the western Pacific margin.. The domain features a west-high-east-low topography, diverse land-cover types, and significant ecosystem variations influenced by climate and elevation. This study considered the following land-cover types in the domain: forests (evergreen needleleaf (ENF), evergreen broadleaf (EBF), deciduous needleleaf (DNF), deciduous broadleaf (DBF), and mixed forests (MF)), grasslands, croplands, savannas, and shrublands, as shown in **Figure 2(b)**. China's vast territory features diverse climatic types. Eastern China experiences a monsoon climate, characterized by cold, dry continental monsoons in winter and warm, humid oceanic monsoons in summer, driving seasonal rainfall patterns. The region is dominated by forests, savannas, grasslands, and croplands. The Tibetan Plateau, with its high altitude and vast area, creates a unique alpine climate. The region is dominated by grasslands and bare soil areas. Northwest China, situated far inland, experiences minimal influence from oceanic monsoons, resulting in an arid climate primarily driven by westerlies. The region is dominated by grasslands and croplands.

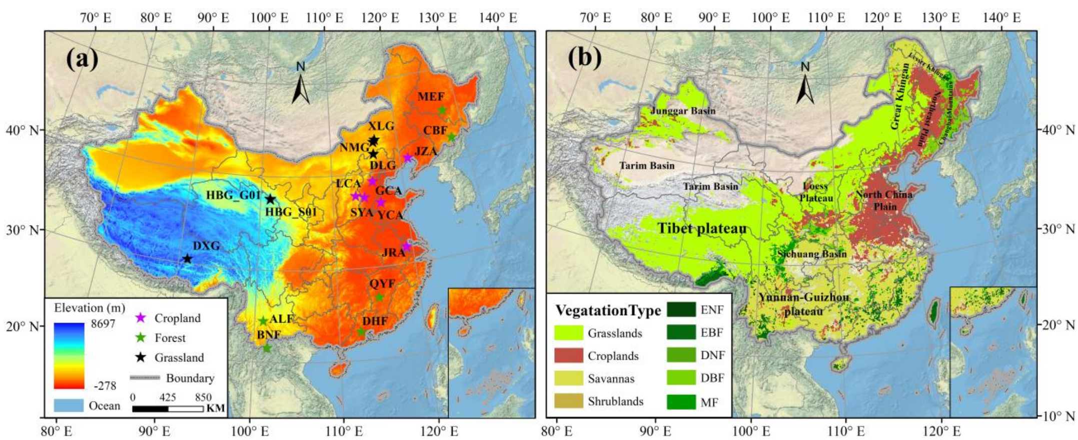

Figure 2. Spatial patterns of (a) elevation and (b) vegetation type in China. The vegetation map only includes the land-cover types analyzed in this study, while blank areas represent land-cover types excluded from the analysis. Vegetation classification follows the MODIS Land-cover type (MCD12Q1) dataset, including forests (ENF, EBF, DNF, DBF, MF), shrublands, savannas, grasslands, and croplands. Elevation data are from the

https://doi.org/10.5194/egusphere-2026-103
Preprint. Discussion started: 29 January 2026

SRTM Digital Elevation Model (Version 4). The basemap is provided by the US National Park Service (https://services.arcgisonline.com/arcgis/services).

2.2 The Noah-MP ensemble

We applied the Noah-MP LSM (Niu et al., 2011; Yang et al., 2011), which represents an improved version of the original Noah LSM. The model features structural enhancements by separating vegetation canopy, snow, and soil into independent layers and incorporating key parameters (He et al., 2023). It adopts a multi-hypothesis framework (Clark et al., 2011), offering multiple parameterization options for key physical processes. The design enhances flexibility and improves performance across diverse environments. Moreover, the multi-parameterization structure enables generating large ensembles by altering certain physical parameterizations. This capability is particularly useful for analyzing the sources of uncertainty.

A 48-member ensemble of Noah-MP (version 5.0) was produced in this study by altering two radiative transfer schemes (MOD, GAP0), three β-factor schemes (NOAHB, CLM, SSiB), two turbulence schemes (M–O, Chen97), and four runoff generation schemes (SIMGM, SIMTOP, NOAHR, BATS). The parameterization schemes are provided in **Table 1**.

The processes considered here were chosen due to their crucial roles in photosynthesis and carbon sequestration in vegetation, as highlighted in previous research. Radiative transfer regulates the energy input for photosynthesis, with optimal light intensity and duration enhancing carbon assimilation (Chen et al., 2012). However, too much radiation exposure can damage the photosynthetic apparatus and a decline in GPP (Misson et al., 2007). β-factor directly controls plant water availability, thus affecting stomatal conductance and photosynthetic efficiency (Wang et al., 2008; Yuan et al., 2007; Schlesinger et al., 1990). Insufficient soil moisture leads to stomatal closure, restricting carbon dioxide uptake and suppressing GPP (Niu et al., 2011). Turbulent processes influence the movement of CO_2 and water vapor between vegetation and the atmosphere, affecting the rate of photosynthetic carbon uptake (Bonan et al., 2018, 2014). Strong turbulence enhances carbon dioxide supply and removes excess water vapor, optimizing photosynthesis and promoting GPP (Zheng et al., 2019). Runoff generation affects soil moisture availability, which in turn influences plant water status (Niu and Yang, 2007). Excessive runoff depletes soil moisture, intensifies water stress, and reduces GPP. In contrast, moderate runoff maintains favorable soil water conditions, sustaining photosynthesis and carbon accumulation (Zheng et al., 2019; Gan et al., 2019; Niu et al., 2011). These processes interact, regulating

https://doi.org/10.5194/egusphere-2026-103
Preprint. Discussion started: 29 January 2026

carbon assimilation and plant productivity, and ultimately determining the carbon sequestration capacity of ecosystems. Besides, this study excluded the radiative transfer scheme 3 (two-stream applied to vegetated fraction, SELLERS, 1985; Dickinson, 1983) of Noah-MP, as it shares the same origin as scheme 1, and may overexpose understory vegetation or snow to solar radiation, potentially causing biased energy partitioning (Niu et al., 2011). Canopy stomatal resistance schemes can also influence GPP simulation, but due to model framework limitations, only the Ball-Berry scheme (Ball et al., 1987) is available. The dynamic vegetation scheme (Yang and Niu, 2003; Dickinson et al., 1998) was activated, and other schemes used default settings.

Table 1

Selected Noah-MP parameterization schemes for the four key physical processes in this study.

Symbol	Physical Process	Options	Notes
RAD	Radiation transfer	1	MOD: Standing for the modified two-stream approach (Niu and Yang, 2004). This improves upon the classical Two-Stream Model.
		2	GAP0: Two-stream with gap=0 (Niu and Yang, 2004). This version assumes no gaps or uneven distribution in the canopy, making it suitable for uniform canopy structures.
BTR	β-factor	1	Noah: The Noah scheme, which focuses on soil moisture (Chen and Dudhia, 2001). The control factor β for transpiration is a function of soil volumetric water content.
		2	CLM: The scheme used in the CLM (Oleson et al., 2010) assumes that the control factor β for transpiration, related to soil moisture, is a function of soil water potential.
		3	SSiB: The scheme used in the SSiB (Xue et al., 1991) also considers the control factor β for transpiration as a function of soil water potential. Compared to the CLM scheme, this model shows a more pronounced response to changes in soil moisture.
SFC	Turbulence	1	M-O: Monin-Obukhov Similarity Theory (Dyer, 1974). This scheme considers zero plane displacement.
		2	Chen97: The scheme used in the Noah LSM (Chen et al., 1997). It does not consider zero-plane displacements but does take into account the difference between thermodynamic roughness and kinetic roughness.
RUN	Runoff generation	1	SIMGM: The scheme used in CLM 4.5 (Niu and Yang, 2007), takes into account the dynamics of groundwater. Runoff is a function of groundwater level, the same as in the TOPMODEL model.
		2	SIMTOP: TOPMODEL with an equilibrium water table (Niu et al., 2005). TOPMODEL Modeling the interaction between groundwater and surface water flow based on soil moisture distribution and hydrologic response.

https://doi.org/10.5194/egusphere-2026-103
Preprint. Discussion started: 29 January 2026

		3	Schaake96: The scheme used in the Noah LSM(Schaake et al., 1996), does not consider groundwater. Runoff is obtained by subtracting soil infiltration from precipitation, which is determined by soil moisture and soil texture.
		4	BATS: The scheme used in the BATS LSM (Yang and Dickinson, 1996), does not consider groundwater. Runoff depends on soil moisture and takes into account a sub-grid distribution of soil moisture saturation zones. Infiltration is the difference between precipitation and runoff.

2.3 CMFD v2.0 forcings

The China Meteorological Forcing Dataset Version 2 (He et al., 2025) (https://doi.org/10.11888/Atmos.tpdc.302088.), including near-surface air temperature, surface pressure, relative humidity, precipitation, downward longwave radiation, and shortwave radiation, was used to force Noah-MP in this study. CMFD v2.0 is a gridded meteorological dataset at high resolution, which combines data from multiple sources: remote sensing, reanalysis, and in-situ observations.. It is specifically developed for land surface process studies in China (Wang et al., 2025; Zhang and Chen, 2025; Bu et al., 2024). Spanning January 1951 to December 2020, the dataset has a three-hourly temporal resolution and a 0.1° spatial resolution.

2.4 Eddy covariance data

Eddy covariance (EC) data were obtained from the Science Data Bank for sites within the ChinaFlux network (https://www.scidb.cn/en), comprising 6 forest sites, 6 grassland sites, and 6 cropland sites (**Table 2**) . High-temporal-resolution flux and meteorological data were logged every half hour across all sites. These datasets underwent rigorous standardization protocols, including quality control checks and post-processing corrections, ensuring high reliability for validating diverse GPP products (Yang et al., 2017).

Table 2

Basic information on the 18 flux sites.

Site	Station name	Longitude (°E)	Latitude (°N)	Vegetation type	Time Range
ALF	Ailaoshan	101.028	24.541	EBF	2009-2013
BNF	Xishuangbanna	101.577	21.614	EBF	2003-2015
CBF	Changbaishan	128.096	42.403	MMF	2003-2010
DHF	Dinghushan	112.534	23.173	EBF	2003-2010

https://doi.org/10.5194/egusphere-2026-103
Preprint. Discussion started: 29 January 2026

MEF	Maoershan	127.668	45.417	DBF	2016-2018
QYF	Qianyanzhou	115.058	26.741	ENF	2003-2010
DLG	Duolun	116.284	42.047	Grassland	2006-2015
DXG	Dangxiong	91.066	30.497	Alpine meadow	2003-2010
HBG_G01	Haibei	101.313	37.613	Alpine meadow	2015-2020
HBG_S01	Haibei	101.331	37.665	Alpine meadow	2003-2013
NMG	Neimenggu	116.404	43.326	Grassland	2003-2010
XLG	Xilin	116.671	43.554	Grassland	2006-2014
GCA	Gucheng	115.735	39.149	Cropland	2020-2022
JRA	Jurong	119.21	31.807	Cropland	2015-2020
JZA	Jinzhou	121.202	41.148	Cropland	2005-2014
LCA	Luancheng	114.413	37.531	Cropland	2013-2017
SYA	Shouyang	113.200	37.750	Cropland	2012-2014
YCA	Yucheng	116.570	36.829	Cropland	2003-2010

2.5 PML-V2 (China) dataset

The Penman-Monteith–Leuning Version 2 (PML-V2) (China) terrestrial ET and GPP dataset (He et al., 2022), obtained from the National Tibetan Plateau Data Center (https://data.tpdc.ac.cn/en/data/40f57c67-33a6-402d-bd37-6ede91919f23/), was used as validation data. This dataset offers daily GPP estimates from February 26, 2000, to December 31, 2020, at a 500 m spatial resolution. Generated via the PML-V2 water-carbon coupled model, the dataset estimates ET and GPP by integrating atmospheric and vegetation data. Specifically, it uses the Penman-Monteith equation for ET and a modified Leuning equation for GPP. Calibrated against 26 eddy covariance flux towers in China, it demonstrates high accuracy, particularly for GPP, outperforming the global PML version (Qian et al., 2024; He et al., 2022). Consequently, it is widely used in ecological research, carbon/water cycle modeling, and evaluation studies (Shi et al., 2024; Huang et al., 2023).

2.6 MODIS LULC dataset

The Moderate Resolution Imaging Spectroradiometer (MODIS) Land Use/Land-cover (LULC) product (MCD12Q1) (https://developers.google.com/earth-engine/datasets/catalog/MODIS_061_MCD12Q1), derived from the MODIS sensors onboard NASA's Terra and Aqua satellites, was used to set the land-cover types in Noah-MP. The dataset

https://doi.org/10.5194/egusphere-2026-103
Preprint. Discussion started: 29 January 2026

offers global land-cover classification on an annual basis at 500 m resolution, covering the period from 2001 to the present. In this study, we employed the LC_Type1 classification scheme from the MCD12Q1 product, which follows the International Geosphere-Biosphere Programme system (Sulla-Menashe and Friedl, 2022). To ensure consistency across all datasets, the land-cover dataset was converted to a 0.1° spatial resolution using interpolation and resampling, aligning with the CMFD dataset grid points. This study used land-cover types from 2001 and did not account for land-cover changes.

2.7 ERA5-Land dataset

The ERA5-Land dataset (https://developers.google.com/earth-engine/datasets/catalog/ECMWF_ERA5_LAND_HOURLY), developed by the European Centre for Medium-Range Weather Forecasts, was used to initialize the land surface states of Noah-MP. This dataset provides a global land surface reanalysis at 0.1° spatial resolution with hourly outputs, spanning from January 1981 to the present.It is generated by integrating a state-of-the-art land surface model with data assimilation, offering a wide range of land surface variables.. ERA5-LAND land surface variables were bilinearly interpolated to the CMFD grid for model initialization.

2.8 SoilGrids 2.0 dataset

In this study, the SoilGrids 2.0 dataset (Poggio et al., 2021) (https://developers.google.com/earth-engine/datasets/catalog/OpenLandMap_SOL_SOL_TEXTURE-CLASS_USDA-TT_M_v02) was used to set soil types in Noah-MP. This dataset provides global soil property predictions at a 250m spatial resolution, which is derived from machine learning-based integration of soil profile observations, remote sensing, and environmental covariates. In this study, we used the United States Department of Agriculture soil texture classification (Soil Survey Staff. 2022). It divides soils into 12 primary classes (e.g., sandy loam, silty clay) depending on the relative amounts of sand, silt, and clay. The soil type was also resampled to a 0.1° resolution, based on the dominant type.

https://doi.org/10.5194/egusphere-2026-103
Preprint. Discussion started: 29 January 2026

3 Methods

3.1 Simulation experiment design

A two-stage spin-up process (Yang et al., 2021; Zheng et al., 2019) was conducted before each of the 48 Noah-MP simulations to establish initial conditions for January 1, 2000 (see Table S1). In the first stage, the atmospheric forcing from 1999 was cycled 30 times. In the second stage, a 1-year forcing period from January 1, 2000, to January 1, 2001, was applied. With a total spin-up period of 31 years, Noah-MP reached equilibrium under all climatic conditions and parameter configurations (Cai et al., 2014).

The subsequent 48 simulations covered the period from 2001 to 2020, using a 15-minute time step. The output frequency is every 8 days. Subsequently, we aggregated the outputs into monthly, seasonal, and annual scales.

3.2 Evaluation metrics

In this study, the Taylor Skill Score (TSS) was employed to provide a concise assessment of the Noah-MP ensemble (Taylor, 2001).

$$\mathrm{TSS} = \frac{4(1+\mathrm{R})}{\left(\hat{\sigma}_f+\frac{1}{\hat{\sigma}_f}\right)^2(1+\mathrm{R}_0)}, \quad (1)$$

where R is a metric for the agreement between observed and simulated time series, and R_0 is the highest correlation among the ensemble simulations. $\hat{\sigma}_f$ is the normalized standard deviation (NSD), which is calculated as the ratio between the standard deviation of observations and that of simulations (see **Equation (4)**). TSS is a metric bounded between 0 and 1, where the upper limit of 1 represents a perfect match between simulation and observation.

To calculate the TSS, R, and NSD were computed. For a model simulation (f) and its corresponding observation (o), the formulas are as follows:

$$\sigma_o = \sqrt{\frac{1}{T}\sum_{t=1}^{T}\left((o_t-\bar{o})\right)^2}, \quad (2)$$

$$\mathrm{R} = \frac{\frac{1}{T}\sum_{t=1}^{T}(f_t-\bar{f})(o_t-\bar{o})}{\sigma_f\sigma_o}, \quad (3)$$

$$\hat{\sigma_f} = \frac{\sigma_f}{\sigma_o} = \frac{1}{\sigma_o}\sqrt{\frac{1}{T}\sum_{t=1}^{T}\left((f_t-\bar{f})\right)^2}, \quad (4)$$

https://doi.org/10.5194/egusphere-2026-103
Preprint. Discussion started: 29 January 2026

where o_t represents the observation value at time step t, $\bar{o}$ is the temporal mean of the observation values, and T is the total time step number. Similarly, f_t denotes the model output at time step t, $\bar{f}$ and $\bar{o}$ are the mean values of the model output (f_t) and observation (o_t), respectively. σ_f and σ_o are their respective standard deviations.

To ensure the diversity and comprehensiveness of evaluation metrics, bias, root-mean-square error (RMSE), and the square of the correlation coefficient (R^2) was also employed, as follows:

$$\text{Bias} = \frac{1}{T}\sum_{t=1}^{T}(f_t - o_t). \tag{5}$$

$$\text{RMSE} = \sqrt{\frac{1}{T}\sum_{t=1}^{T}\left[\left(f_t - \bar{f}\right) - \left(o_t - \bar{o}\right)\right]^2}, \tag{6}$$

A positive bias indicates an overestimation by Noah-MP compared to PML GPP, while a negative bias indicates an underestimation. Since RMSE quantifies the average error magnitude, values nearer to 0 therefore serve as a direct indicator of superior simulation accuracy.. R^2 corresponds to the square of the R and indicates how well the Noah-MP model fits the observations.

3.3 Sobol' total sensitivity index

To determine which physical processes exert the greatest control on GPP, we utilized the Sobol' total sensitivity index (Saltelli et al., 2010; Sobol', 2001; Saltelli and Sobol, 1995). The Sobol' total sensitivity index (S_P) is defined as:

$$S_\wedge = \frac{E_{\sim\wedge}(V_\wedge(Y|\sim\wedge))}{V(Y)}, \tag{7}$$

where $S_\wedge$ denotes the Sobol' total sensitivity associated with the schemes of a specific process $\wedge$; $\sim\wedge$ represents all processes except $\wedge$; Y refers to the 48 Noah-MP model outputs, which include both multi-year means and seasonal averages; $V(Y)$ represents the variance among the 48 outputs; $V_\wedge(Y|\sim\wedge)$ measures the variance induced by the $\wedge$ schemes, and $E_{\sim\wedge}$ is the average across all other parameterization combinations.

The Sobol' total sensitivity index measures the proportion of variance in model outputs attributable to the parameterization of process $\wedge$, relative to the total ensemble variance. This

https://doi.org/10.5194/egusphere-2026-103
Preprint. Discussion started: 29 January 2026

index is scaled between 0 and 1, where 0 indicates that ∧'s parameterization has no impact on the simulations, while 1 denotes complete control of the simulations by ∧. A higher value denotes a greater degree of dependence of the simulations on ∧.

4 Results

4.1 Evaluation of the Noah-MP ensemble

To comprehensively assess Noah-MP's performance in simulating GPP across 48 physics configurations, we adopted a two-tier validation approach. First, site-level evaluations leveraged eddy covariance flux tower observations at selected sites. This approach supports process-oriented assessment of model accuracy under diverse environmental and vegetation conditions. Second, regional-scale evaluations utilized the remote-sensing-based PML-GPP dataset. This provides spatially continuous estimates, enabling assessment of the model's performance to capture broad-scale spatial patterns and interannual variability, serving as a complementary and independent benchmark to site-level observations.

4.1.1 Site-Based Validation Using Eddy Covariance Flux Towers

The site-level performance of Noah-MP was examined by comparing model outputs with observations from individual flux tower sites. Figure 3 shows a boxplot representing the distribution of TSS (max, min, median) from 48 site-level simulations.

Median TSS values consistently exceeded 0.50 at all cropland sites. For forest sites, TSS and R^2 exceeded 0.50 at all sites except DHF. In contrast, both TSS and R^2 values were generally below 0.60 at grassland and cropland sites. Specifically, the median TSS values at LCA, SYA, and YCA sites were greater than 0.80, while those at ALF, MEF, and JRA ranged between 0.60 and 0.80. The DHF site and all grassland sites had median TSS values below 0.50, indicating limited GPP simulation capabilities at these locations as demonstrated by the notably low TSS.

The TSS range reflects the performance variability among different ensemble members. As shown in **Figure 3**, forest sites exhibited relatively small ensemble spreads, suggesting consistent performance across ensemble members. In contrast, all grassland sites showed large ensemble spreads. Among cropland sites, both GCA and JZA exhibited substantial TSS variability. These findings reveal considerable model performance divergence in grassland and

https://doi.org/10.5194/egusphere-2026-103
Preprint. Discussion started: 29 January 2026

cropland ecosystems, under different parameterization schemes. In forest ecosystems, however, the model exhibited excellent performance with low sensitive to parameterizations choices, suggesting greater robustness across ensemble members.

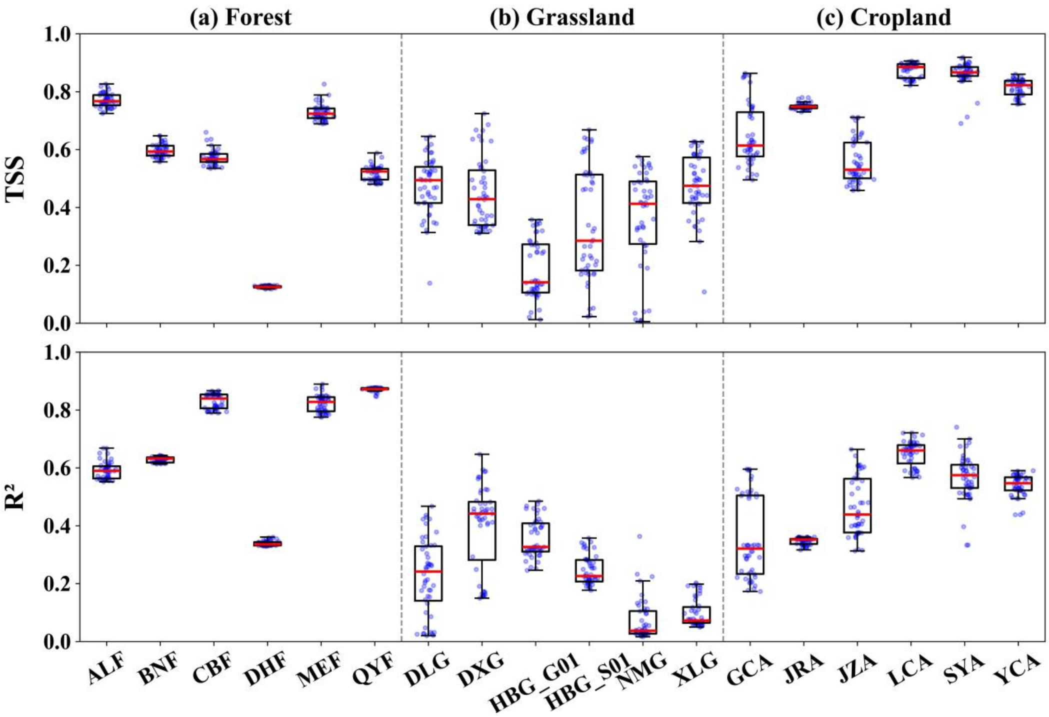

Figure 3. Taylor skill score (TSS) and squared correlation coefficient (R^2) evaluating Noah-MP simulated GPP against site-level observations across 48 ensemble experiments. Box plots represent the distribution of results from 48 ensemble experiments, showing the minimum, first quartile, median, third quartile, and maximum values.

4.1.2 Spatial Validation Using the PML GPP Dataset

To further evaluate the spatial representativeness of Noah-MP simulated GPP, we conducted a spatial comparison with the PML-GPP product. **Figure 3** presents the spatial distribution and seasonal variations of GPP across China from two sources: the PML dataset (**Figures 3a, c, e, g, i, k**), serving as reference data, and the Noah-MP multi-physics ensemble mean (**Figures 3b, d, f, h, j, l**). Both datasets revealed clear seasonal GPP patterns, characterized by summer peaks and winter valleys, highlighting climate phenology carbon uptake. In spring, GPP in China showed a northwest-to-southeast increasing gradient, reaching highest values appearing in the central and lower Yangtze River Basin. During summer, GPP reached its peak

https://doi.org/10.5194/egusphere-2026-103
Preprint. Discussion started: 29 January 2026

in the high-productivity zones, including eastern, southern, and northeastern China, probably attributed to favorable radiation, temperature, and precipitation conditions. In autumn, GPP declined along a southeast-to-northwest gradient. During winter, photosynthetic activity was minimal, with near-zero GPP in northern and high-altitude regions, while southern China maintained modest productivity. The multi-year mean GPP follows hydroclimatic patters: highest in warm-humid southeast, lowest in cold-arid northwest. Vegetation growth is promoted by sufficient water and heat in water-rich regions, whereas in water-limited regions, extreme temperatures and scarcity of moisture often constrain vegetation productivity (Piao et al., 2013). **Figures 3k** and **3l** show GPP variations across different vegetation types. Forests, croplands, and savannas exhibited relatively higher GPP, while grasslands and shrublands showed lower GPP. Vegetation exhibiting lower productivity is generally located in the northern drylands, where both moisture and temperature act as constraints (Li et al., 2023; Qiu et al., 2020). Additionally, GPP across different vegetation types is determined not only by climatic hydrological drivers but also by the physiological characteristics of the species (Waring et al., 1998; Reich et al., 1997).

https://doi.org/10.5194/egusphere-2026-103
Preprint. Discussion started: 29 January 2026

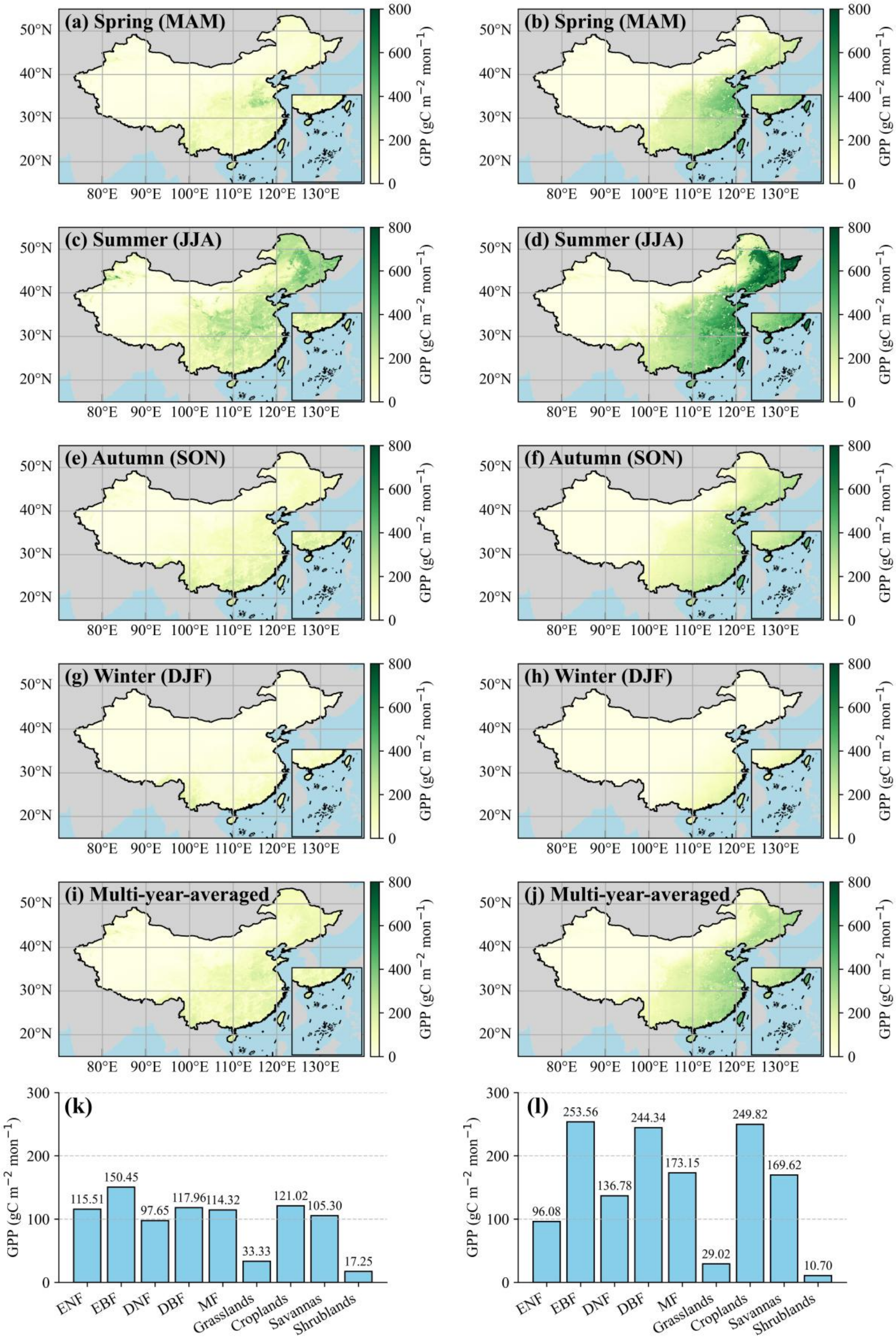

397

https://doi.org/10.5194/egusphere-2026-103
Preprint. Discussion started: 29 January 2026

Figure 4. Spatial distribution of GPP for different seasons and the multi-year mean. The left column presents the GPP distribution derived from the PML dataset, while the right column shows the ensemble mean GPP distribution from the Noah-MP model.

Monthly biases of the Noah-MP ensemble mean, compared to the PML dataset across vegetation types, are depicted in **Figure 5**. The results revealed substantial variability in monthly GPP bias. Grasslands and shrublands exhibited minimal biases, whereas EBF and croplands displayed notably larger positive biases, particularly during the growing season. The overestimation was more pronounced in high-productivity ecosystems in eastern China, which have substantial carbon sequestration capacity. The underlying causes of these discrepancies, especially in high-productivity seasons and regions, need further exploration.

https://doi.org/10.5194/egusphere-2026-103
Preprint. Discussion started: 29 January 2026

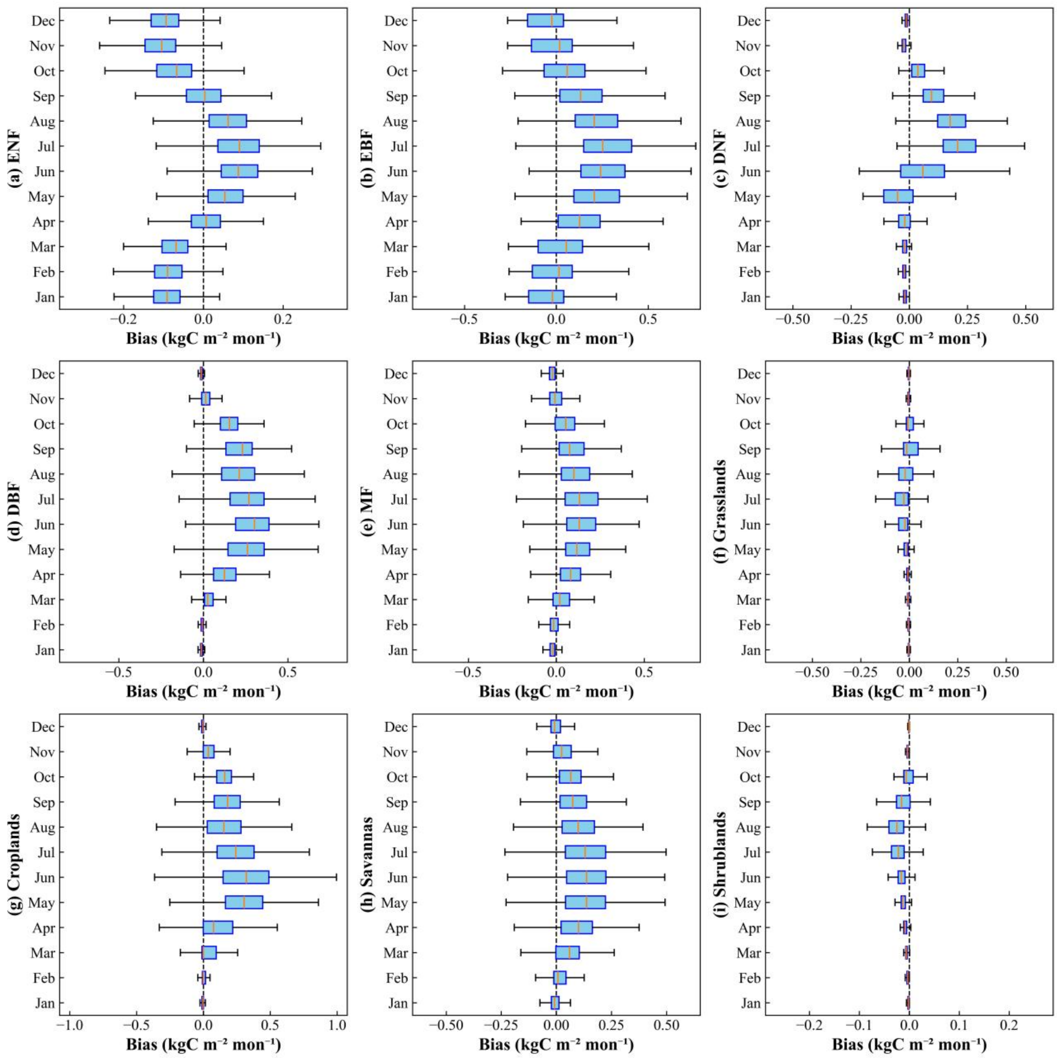

Figure 5. Monthly bias of Noah-MP ensemble mean GPP across vegetation types. The box show pixel-level variability and red lines indicate the mean.

4.2 Physical process sensitivity

Figure 6 presents the spatial pattern of the Sobol' sensitivityof the four physical processes at multi-year and seasonal scales. Focusing on the multi-year scale, radiation transfer exhibited the highest sensitivity on the Tibetan Plateau. Across most Chinese regions excluding the Tibetan Plateau and the western part of the Yunnan-Guizhou Plateau, GPP showed the highest sensitivity to the β-factor, indicating that water availability is the main factor limiting carbon assimilation. The turbulence process showed low sensitivity to GPP simulation. The runoff generation schemes showed slight sensitivity across China, particularly in the Hai River Basin, Huai River Basin, and the Yunnan-Guizhou Plateau.

The Tibetan Plateau and northeastern Inner Mongolia exhibited the strongest GPP response to changes in radiation transfer (**Figure 6a**). Theoretically, in such radiation-rich environments, radiation transfer should not be the dominant limiting factor for GPP. However, Figure S2 reveals substantial differences in APAR (and thus GPP) between the RAD01 and RAD02 parameterization schemes across these areas. This discrepancy primarily arises from RAD01 incorporating vegetation gap effects in radiation transfer calculation, while RAD02 does not (Niu and Yang, 2004). For densely forested canopies with closed structures (Fig. S3-S7), differences between the two schemes are relatively small. In contrast, grasslands and sparse shrubs are the predominant vegetation types across the Tibetan Plateau and northeastern Inner Mongolia, where vegetation aggregation and gap distribution are more pronounced, thereby amplifying differences in canopy radiation transfer.

GPP simulations were more strongly influenced by the β-factor across most Chinese regions, particularly the northern arid and semi-arid areas (**Figure 6b**). These regions are characterized by abundant available energy, but are primarily constrained by water availability. During spring and summer, increased ET intensified soil moisture stress, with the β-factor critically regulating GPP. This water-driven effect was predominantly observed in Northwest China and the Songliao Plain. In Northwest China, low precipitation made water the primary constraint on carbon assimilation. Similarly, in the Songliao River Basin, a key Chinese agricultural zone, high crop water demand, meant droughts substantially affected GPP dynamics. Although winter vegetation dormancy reduced GPP, the β-factor remained sensitive due to its "lag effect" on soil moisture, which influenced vegetation recovery in the subsequent spring (Knapp et al., 2008; Schwinning and Sala, 2004). As other processes showed low sensitivities in winter, the sensitivity of the β-factor became particularly pronounced.

At the multi-year scale, turbulence exhibited low sensitivity to GPP across most of China, with detectable effects confined to the forested area in eastern Northeast China. This is primarily because turbulence operates as a short-term micrometeorological process that typically fluctuates at sub-hourly to hourly timescales (Baldocchi, 2003). In addition, ecosystems such as grasslands,

https://doi.org/10.5194/egusphere-2026-103
Preprint. Discussion started: 29 January 2026

croplands, and savannas usually exhibit weak vertical gradients of CO_2 and water vapor, making them less dependent on turbulent mixing. In contrast, forest ecosystems in eastern Northeast China are characterized by tall and dense canopies, where pronounced vertical stratification requires effective turbulent transport to facilitate the transfer of gases from the canopy to the atmosphere (Stoy et al., 2006).

Runoff generation exhibited high sensitivity in China's eastern regions, particularly in the Hai River Basin, the Huai River Basin, and Yunnan Province, with consistent spatial patterns inall seasons except winter. In Yunnan Province, runoff generation is most sensitive in spring. Yunnan's complex terrain and uneven water distribution make runoff vital for water redistribution during dry seasons (Winkler et al., 2018; Immerzeel et al., 2010). The region's warm climate and high elevation cause early spring snowmelt, which boosts soil moisture and supports timely vegetation growth (Barnett et al., 2005). Runoff generation is most sensitive in summer in the Hai River Basin and Huai River Basin. In these basins, concentrated summer precipitation and irrigation are crucial for maintaining cropland GPP during drier periods. During winter, the sensitivity weakened and was largely restricted to southern regions. Winter precipitation reduction and vegetation dormancy decreased runoff sensitivity to GPP simulations, yet some regions in southern China remained sensitive as winter soil moisture and water availability affected spring vegetation recovery.

Soil moisture stress (β-factor) and radiation transfer were the main limiting factors for GPP in dry regions, including Northwest China. By contrast, in wet regions such as southern China,, runoff generation and turbulence seasonally regulated carbon assimilation. During peak growth periods (spring and summer), radiation transfer and soil moisture stress more strongly impacted GPP, increasing sensitivity. Although GPP was low in winter, soil moisture stress still impacted model outputs in eastern Inner Mongolia and Northwest China by influencing vegetation recovery, showing notable seasonal lag effects.

https://doi.org/10.5194/egusphere-2026-103
Preprint. Discussion started: 29 January 2026

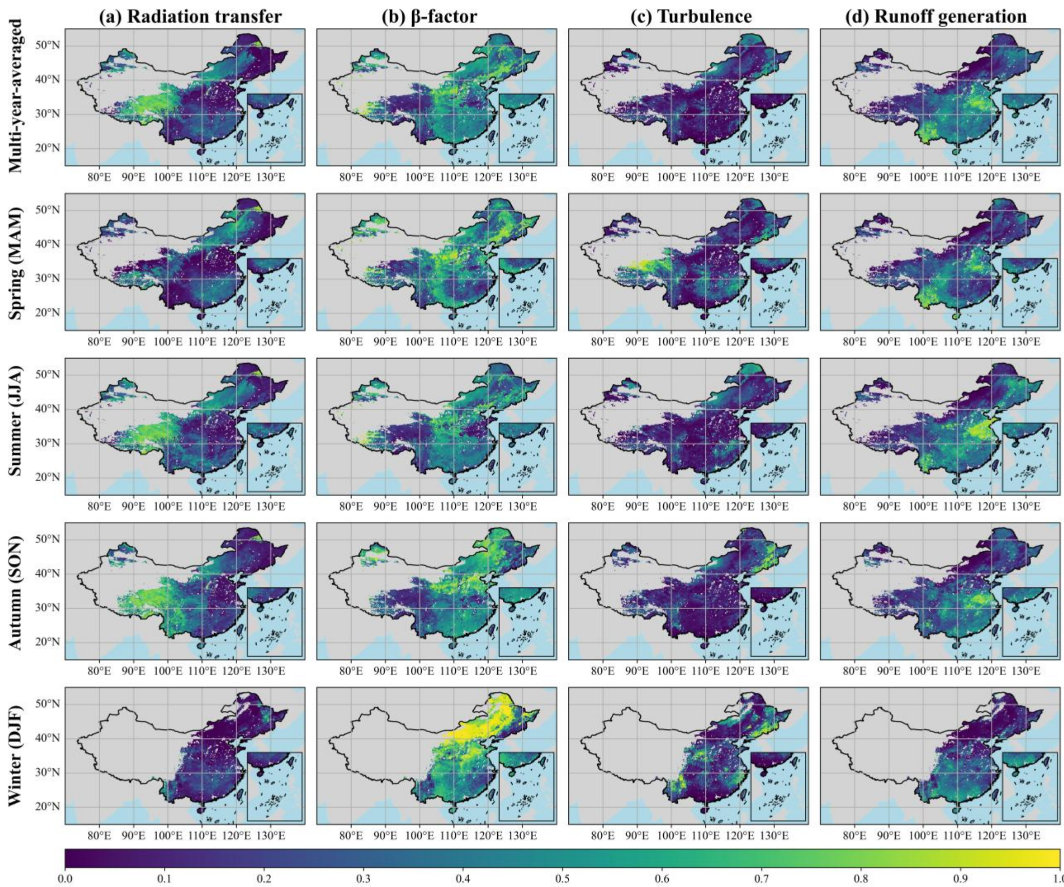

Figure 6. The Sobol' index of the Noah-MP ensemble-simulated multi-year-averaged and seasonal GPP to the four physical processes (i.e., radiation transfer, β-factor, turbulence, and runoff generation). Notably, blank areas represent regions with zero GPP under all 48 simulation schemes due to a lack of vegetation cover, making it impossible to assess sensitivity.

Figure 7 shows the seasonal patterns of the processes exerting the strongest control on GPP. As in **Figure 6**, radiation transfer was dominant process over the Tibetan Plateau at the multi-year scale as well as in summer and autumn while winter GPP in this region dropped to nearly zero. The β-factor dominated in the water-limited regions (i.e., northwest China, the Northeast Plain, and parts of southern China), reflecting its broad significance. Runoff mostly affected Yunnan and the North China Plain. Turbulence was the key influence in high-elevation forest areas (i.e., Changbai Mountains forest region) in spring and winter.

Spatially, the dominant factors controlling GPP exhibit significant spatial variability across China. At multi-year scales, radiation transfer was the primary controlling factor of GPP

https://doi.org/10.5194/egusphere-2026-103
Preprint. Discussion started: 29 January 2026

in the northeastern Inner Mongolia and Tibetan Plateau. This mainly results from the divergent performance of radiation schemes in grasslands and sparse shrubs (Figs. S2). The β-factor was particularly influential in most regions of China. In the arid northwest and northeast, as well as southern regions with seasonal water shortages, low soil moisture limited GPP, making the β-factor a key control, as water scarcity reduced photosynthetic efficiency. In high-elevation forest regions such as the Lesser Khingan and Changbai Mountains, turbulent heat flux plays a key role in regulating GPP, especially during cold seasons. Turbulent heat exchange helps maintain canopy temperatures above freezing, thereby extending the photosynthetic period (Bonan et al., 2018; Ensminger et al., 2006). In areas with enclosed terrain, including valleys and basins, turbulence mitigates the buildup of cold air, making this effect more noticeable (Wang et al., 2016).. Runoff played a dominant role in southwestern and eastern China, where complex terrain and uneven precipitation led to increased sensitivity to GPP in areas like river basins.

The dominant processes controlling GPP varied significantly across the four seasons. Turbulence became more influential in spring, dominating GPP dynamics in the Tibetan Plateau, Changbai Mountains, and parts of central and eastern China. Rising temperatures and winds increased surface heating and atmospheric instability, enhancing turbulence. As plants enter their growing season with higher CO_2 demand, turbulence enhances gas exchange, boosting photosynthesis and thus increasing its impact on GPP (Baldocchi, 2014; Finnigan, 2000). In summer, the distribution of dominant physical processes closely resembled the multi-year average, likely because the Noah-MP ensemble showed the largest spread during summer. In autumn, the main processes in the Yunnan-Guizhou Plateau shifted from runoff generation to radiation transfer. Runoff generation was less impactful due to reduced rainfall and smaller runoff differences. Solar radiation became the main limiting factor (Wang et al., 2023). When radiation levels were sufficiently high, photosynthetic activity stayed high. In winter, the β-factor was the main driver of GPP, while radiation had minimal effect. This is because low temperatures suppress vegetation activity, making radiation less sensitive to GPP changes (Fu et al., 2017). Conversely, in regions with winter-spring dry seasons like Southwest China, soil moisture becomes the dominant control on GPP (Zhou et al., 2019).

Overall, the dominant physical processes controlling GPP exhibit both seasonal and spatial variability. Spatially, radiation transfer was the primary driver of GPP on the Tibetan Plateau, while the β-factor, which represents vegetation stomatal response to soil moisture,

https://doi.org/10.5194/egusphere-2026-103
Preprint. Discussion started: 29 January 2026

played a dominant role across most other regions of China, including the northwest, the Northeast Plains, and parts of southern China. Notably, the β-factor is the principal control on GPP throughout most of the year, particularly in winter, when its influence extends nearly the whole of China. During spring and winter, turbulence primarily affects GPP, whereas in summer, runoff generation plays a larger role; overall, the β-factor remains the key driver..

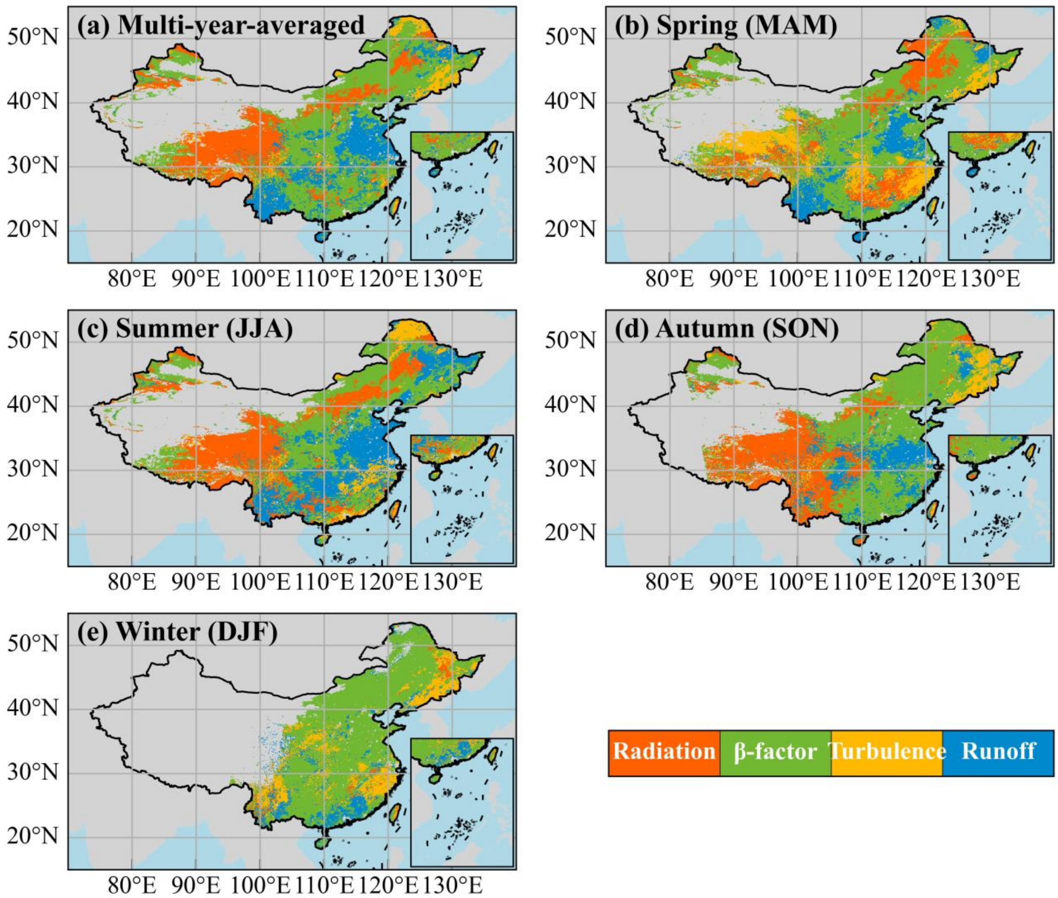

Figure 7. Spatial distributions of the dominant physical process for the Noah-MP ensemble-simulated multi-year-averaged and seasonalGPP.

4.3 Parameterization scheme optimization across different vegetation types

To determine the best parameterization scheme for dominant physical processes in GPP simulations across different vegetation types, we analyzed the process with the highest Sobol' sensitivity index for each vegetation type. Figure 8 presents the total Sobol' sensitivity indices of

https://doi.org/10.5194/egusphere-2026-103
Preprint. Discussion started: 29 January 2026

Noah-MP-simulated GPP (multi-year average and seasonal) for four physical processes across vegetation types. These variations suggest that the dominant processes governing GPP differ depending on the balance between water and energy limitations.

The sensitivity of GPP simulations to key physical processes varied significantly across vegetation types, with shrubland ecosystems being most sensitive to the radiation transfer process (**Figure 8**). Shrublands, widely distributed in arid regions and the eastern Tibetan Plateau, exhibited high sensitivity to radiation transfer (index = 0.92), but showed minimal sensitivity to the β-factor, turbulence, and runoff generation. The RAD process directly influences the amount of shortwave radiation absorbed by vegetation (SAV) and the absorbed photosynthetically active radiation (APAR). As shown in **Figure S8**,simulations using the RAD01 scheme produced greater SAV and APAR values. In the Noah-MP model, the radiation process indirectly regulates vegetation growth and leaf area index (LAI) by modulating photosynthesis, which mainly depend on solar radiation and canopy PAR absorption. Consequently, the simulated LAI and fraction of vegetated area (FVEG) varied significantly across different radiation transfer schemes. The results suggest that the RAD01 scheme yields more realistic simulations and better aligning with actual conditions.

The β-factor process exhibited the highest sensitivity in GPP simulations over ENF, savannas, croplands, and grasslands (**Figure 8**). Although all β-factor parameterization schemes regulate photosynthetic and transpiration through modulating stomatal resistance, their performance varied substantially among ecosystem. Specifically, in ENF ecosystems, all three schemes showed a sharp increase in transpiration rate starting around DOY 60, quickly reaching a peak (**Figure S9**). Meanwhile, APAR exhibited a bimodal pattern, resulting in simulated GPP to peak earlier than observations. For savannas and croplands, the differences among the three schemes were minor but schemes systematically overestimated GPP. In grassland ecosystems, although the BTR03 scheme significantly enhanced the simulated APAR and transpiration rate, GPP was still substantially underestimated. These findings demonstrate systemic limitations in current β-factor parameterizations across different ecosystems, as even the most favorable scheme fails to accurately capture ecosystem-specific GPP dynamics.

The turbulence process exhibited, the highest Sobol' sensitivity index of GPP in DBF ecosystems. Noah-MP simulations revealed that the surface exchange coefficient directly

https://doi.org/10.5194/egusphere-2026-103
Preprint. Discussion started: 29 January 2026

influences the vegetation-atmosphere exchanges of sensible and latent heat flux. The SFC01 scheme generated higher sensible heat flux and turbulent exchange coefficients than to the SFC02 scheme, whereas SFC02 resulted in relatively higher latent heat values (**Figure S10**). Despite the substantial differences in energy flux simulations between the two schemes, their simulated GPP values differed only slightly. Compared with observations, both schemes showed systematic GPP overestimation, suggesting that vegetation energy-use efficiency may be overrepresented in the model.

The runoff generation process exhibited the highest sensitivity in GPP simulations for EBF, DNF, and MF (**Figure 8**). Different runoff parameterization schemes alter the partitioning of surface and subsurface runoff, which in turn modifies soil moisture conditions and drives differences in simulated vegetation dynamics, including LAI, fraction of vegetated area (FVEG), and ultimately GPP (**Figure S11**). The impact of runoff generation parameterizations on GPP is primarily mediated through changes in soil moisture. However, the four runoff generation schemes produced similar GPP simulations, with only minor differences relative to observed GPP. Moreover, all Noah-MP scheme combinations systematically overestimated GPP. These results suggest that further refinement of model parameterizations is necessary to improve the accuracy of GPP simulations.

This systematic analysis reveals distinct ecosystem-dependent controls on GPP simulations in Noah-MP. Among the key physical processes, the radiation transfer scheme dominates in shrublands, with RAD01 performing best due to its better capturing radiation absorption (SAV/APAR) and subsequent vegetation dynamics (LAI/FVEG) (**Table S2, S3**). For β-factor, while exhibiting high sensitivity across ENF, savannas and croplands, all current schemes show critical limitations - even the optimal BTR03 scheme substantially underestimates GPP. The turbulence process proves most influential in DBF ecosystems, though both SFC01 and SFC02 similarly overestimate GPP, suggesting fundamental issues in energy-carbon coupling. Similarly, for runoff generation processes in tropical/temperate forests, all four parameterizations produce comparable but consistently overestimated GPP results. Importantly, these systematic biases across multiple ecosystems indicate the model's inherent tendency to overestimate vegetation resource use efficiency. These findings collectively underscore the need for: (1) adopting RAD01 for shrubland simulations, (2) comprehensive recalibration of energy-

https://doi.org/10.5194/egusphere-2026-103
Preprint. Discussion started: 29 January 2026

water-carbon coupling mechanisms across all ecosystems to reduce persistent overestimation biases.

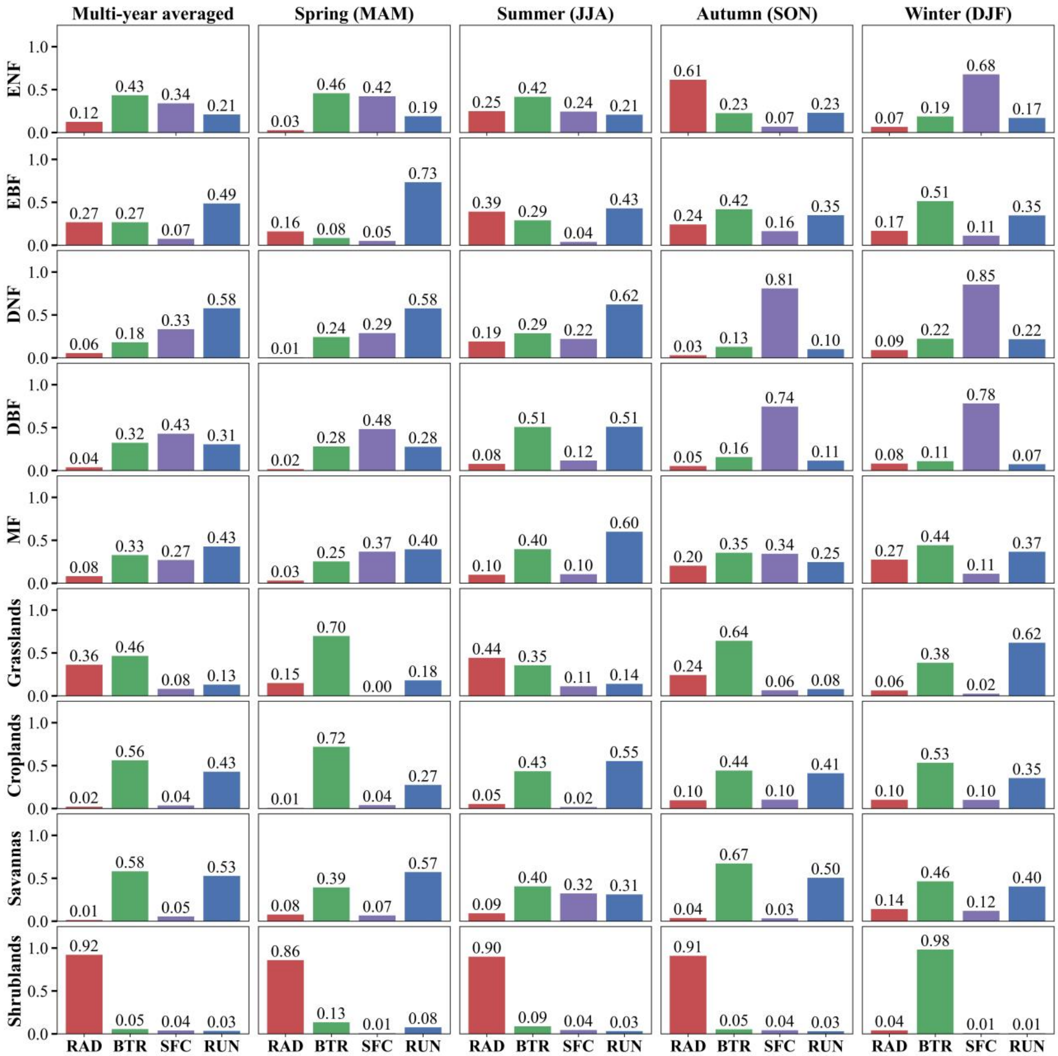

Figure 8. The Sobol' index of the Noah-MP ensemble-simulated multi-year-averaged and seasonal GPP to the four physical processes across different vegetation types. Here, RAD denotes radiation transfer, BTR denotes the β-factor, SFC denotes turbulence, and RUN denotes runoff generation.

5 Conclusions and discussion

We examined the performance of the Noah-MP ensemble with multiple parameterizations in reproducing GPP, based on flux tower measurements and PML GPP datasets. The Noah-MP ensemble was generated by perturbing parameterization schemes of four

https://doi.org/10.5194/egusphere-2026-103
Preprint. Discussion started: 29 January 2026

key physical processes: radiation transfer, turbulence, the β-factor, and runoff generation. In China, GPP showed significant spatial-temporal variation, with spring/summer as peak seasons and southeastern/northeastern regions acting as major carbon sinks. Vegetation type greatly shaped GPP, with forests being the largest carbon contributors, while grasslands and shrublands exhibited lower productivity. The Noah-MP effectively captured the spatiotemporal patterns of GPP, but overestimated forest and cropland GPP in peak seasons, potentially due to underestimating the photosynthesis inhibition under soil moisture deficits. The model exhibited strong performance across most Chinese ecosystems, with moderate accuracy in shrublands, and notably inferior results in evergreen forest, demonstrating its applicability in GPP simulation for Chinese terrestrial ecosystem.

Our results align with Arsenault et al.(2018), indicating that Noah-MP overestimates GPP throughout the growing season, notably in forests and croplands. This overestimation likely arises from the model's insufficient response to water stress and stomatal regulation under drought conditions, which leads to the overestimation of carbon assimilation rates. Additionally, limitations in phenology-related parameterizations and the dynamic vegetation module might lead to excessive carbon allocation to photosynthetic organs, such as buds in spring (Ma et al., 2017; Niu et al., 2011). Addressing current model limitations requires advancing carbon allocation schemes, refining photosynthetic temperature regulation, and integrating nutrient constraints, with an emphasis on nitrogen, within vegetation processes (Gim et al., 2017; Cai et al., 2016; Schaefer et al., 2012; Stöckli et al., 2008).

With the Noah-MP ensemble, the Sobol' total sensitivity index was applied to determine the impact of major physical processes on GPP in China's terrestrial ecosystems. China's ecosystem GPP was influenced by multiple processes, showing spatial heterogeneity. In arid regions like Northwest China, the β-factor (soil moisture stress) and radiation transfer limited GPP, while in humid southern China, runoff generation and turbulence regulated carbon assimilation. During peak growth periods, radiation transfer and the β-factor strongly impacted GPP. For different ecosystems, water-related factors, including the β-factor and runoff generation, mainly influenced cropland and savanna GPP, while radiation transfer and turbulence affected shrublands and forests respectively. GPP's dominant processes varied seasonally and spatially, with the the β-factor dominated in most Chinese regions and radiation transfer showed stronger control on the Tibetan Plateau. Except in summer, the β-factor was the main GPP driver,

https://doi.org/10.5194/egusphere-2026-103
Preprint. Discussion started: 29 January 2026

especially in winter. In spring, there are no obvious limiting factors, except for a slight sensitivity exhibited by turbulence; in summer, both radiation transfer and runoff generation show moderate influence on GPP; in autumn, the dominant process was radiation transfer.

The sensitivity of physical process parameterizations is critical for identifying the primary drivers and mechanisms underlying the spatiotemporal variations of GPP. In spring, turbulence significantly influences GPP by modulating surface energy fluxes, which in turn regulate vegetation–atmosphere gas exchange and surface temperature (Misson et al., 2007). Specifically, turbulent transport of heat and moisture helps maintain canopy temperatures above freezing and enhances carbon dioxide exchange efficiency, thereby extending the active photosynthetic period (Misson et al., 2007). Additionally, turbulence mitigates cold air accumulation in topographically enclosed areas such as valleys and basins, further supporting microclimatic conditions favorable for vegetation growth (Ensminger et al., 2006). In China's arid and semi-arid regions, including the Northwest and Northeast Plain, the β-factor exerted a pronounced influence on autumn and winter GPP (Kannenberg et al., 2024), emphasizing the critical influence of soil moisture availability on transpiration and carbon uptake in these water-limited ecosystems, aligning with previous findings (Wang et al., 2023; Zheng et al., 2019; Nelson et al., 2018; Wolf et al., 2016). Runoff played a significant role in controlling GPP in humid regions, including the Yunnan-Guizhou Plateau and eastern China. It impacts photosynthetic efficiency by altering surface and subsurface water availability (Lei et al., 2014). Incorporating detailed runoff-soil moisture interactions and vegetation-specific hydrological processes may enhance simulation accuracy in these regions. Overall, GPP variability in China arose from complex interactions of climatic drivers, vegetation types, and ecosystem-specific physiology. This highlights the need for model improvements in simulating radiation transfer, soil moisture transport, and vegetation dynamics to reduce uncertainties. Notably, sensitivity patterns varied regionally even within the same vegetation type, reflecting local climate and hydrological influences. Such spatial heterogeneity indicates the importance of conducting region-specific modeling and implementing targeted management, such as optimizing water resources in arid areas and boosting light-use efficiency in humid regions.

Based on systematic model performance evaluations and parameterization scheme sensitivity analyses, this study proposes optimized Noah-MP model configurations for terrestrial ecosystems in China. The findings indicate that the modified two-stream approximation scheme

https://doi.org/10.5194/egusphere-2026-103
Preprint. Discussion started: 29 January 2026

(RAD01) exhibits superior performance in simulating radiation transfer processes, particularly showing significant advantages in grasslands and shrubland ecosystems. For β-factor, while the three β-factor schemes show minimal differences across most vegetation types, BTR03 demonstrates relatively better performance in cropland ecosystems. Importantly, both surface exchange (SFC01/SFC02) and runoff parameterizations consistently overestimate GPP without showing substantial inter-scheme performance variations. Consequently, we recommend: (1) adopting RAD01 for radiation transfer simulations, (2) prioritizing BTR03 for cropland applications, and (3) focusing on fundamental improvements in energy-carbon coupling and hydro-vegetation interaction mechanisms to address the identified systematic biases and enhance overall model accuracy.

This study assessed the ability of Noah-MP to simulate GPP across Chinese ecosystems, explored key physical processes shaping GPP variations, and offered optimal parameterization scheme recommendations for GPP modeling. The findings contribute to improving ecosystem carbon uptake modeling and support the improvement of carbon management strategies. However, several limitations warrant attention in future work:

(1) Parameterization schemes limitations: only a subset of parameterization schemes was included due to computational constraints, with other parameters and parameterization schemes remaining not considerated. Future research should expand the ensemble by incorporating more parameters and schemes related to vegetation carbon sequestration, such as canopy height and rain-snow partitioning schemes. Furthermore, plant physiology-related processes, like plant hydraulics, were not incorporated in the Noah-MP 5.0 version used (Li et al., 2021). Subsequent research is needed to include these processes and evaluate their influence on GPP. (2) Validation data uncertaintie: though the PML GPP (China) dataset used here was deemed superior by prior studies, it still deviates from site observations. The PML GPP shows strong agreement with flux tower observations, with an NSE of 0.82 and an RMSE of 1.71 g C m^{-2} d^{-1} (He et al., 2022). (3) Model structural constraints: current physical process models like Noah-MP simplify the parameterization of vegetation carbon fluxes, introducing uncertainties in GPP simulation. Integrate data assimilation and machine-learning-based modeling can effectively reduce such uncertainties and enhance simulation accuracy.

Acknowledgment

https://doi.org/10.5194/egusphere-2026-103
Preprint. Discussion started: 29 January 2026

This work was funded by the National Key Research and Development Program of China (Grant No. 2022YFF1300501), the Natural Science Foundation of Liaoning Province (Grant No. 2024-BSBA-62), the Open Research Fund Project of Key Laboratory of Ecosystem Carbon Source and Sink, China Meteorological Administration (Grant No. ECSS-CMA202305), the Fundamental Research Funds of the Chinese Academy of Meteorological Sciences (Grant No. 2024Z001).

Data availability statement

All public datasets used in this study (including CMFD, PML-V2, MCD12Q1, ERA5-Land, and SoilGrids 2.0) were obtained from their respective official sources cited in the article. The source code and simulated data generated in this study have been uploaded to Zenodo (https://doi.org/10.5281/zenodo.18158937, Lai, 2026).

CRediT authorship contribution statement

J.L. conceived the study, processed and analyzed the data, and wrote the original draft. W.F. and J.W. secured funding, supervised the project, and contributed to conceptualization and manuscript revision. A.W., Y.L., L.S., Y.Z., Y.D., R.C., and R.L. participated in reviewing and editing the manuscript. All authors contributed to the final version and approved its submission.

Declaration of competing interest

The authors declare no conflicts of interest.

References

Arsenault, K.R., Nearing, G.S., Wang, S., Yatheendradas, S., Peters-Lidard, C.D., 2018. Parameter Sensitivity of the Noah-MP Land Surface Model with Dynamic Vegetation. Journal of Hydrometeorology 19, 815–830. https://doi.org/10.1175/jhm-d-17-0205.1

Baker, I., Denning, A.S., Hanan, N., Prihodko, L., Uliasz, M., Vidale, P.-L., Davis, K., Bakwin, P., 2003. Simulated and observed fluxes of sensible and latent heat and CO2 at the WLEF-TV tower using SiB2.5. Global Change Biology 9, 1262–1277. https://doi.org/10.1046/j.1365-2486.2003.00671.x

Baldocchi, D., 2014. Measuring fluxes of trace gases and energy between ecosystems and the atmosphere – the state and future of the eddy covariance method. Global Change Biology 20, 3600–3609. https://doi.org/10.1111/gcb.12649

Baldocchi, D.D., 2003. Assessing the eddy covariance technique for evaluating carbon dioxide exchange rates of ecosystems: past, present and future.

Ball, J.T., Woodrow, I.E., Berry, J.A., 1987. A Model Predicting Stomatal Conductance and its Contribution to the Control of Photosynthesis under Different Environmental Conditions, in: Biggins, J. (Ed.), Progress in Photosynthesis Research: Volume 4 Proceedings of the VIIth International Congress on Photosynthesis Providence, Rhode Island, USA, August 10–15, 1986. Springer Netherlands, Dordrecht, pp. 221–224. https://doi.org/10.1007/978-94-017-0519-6_48

https://doi.org/10.5194/egusphere-2026-103
Preprint. Discussion started: 29 January 2026

Barnett, T.P., Adam, J.C., Lettenmaier, D.P., 2005. Potential impacts of a warming climate on water availability in snow-dominated regions. Nature 438, 303–309. https://doi.org/10.1038/nature04141

Bonan, A.G., 1996. A Land Surface Model (LSM Version 1.0) for Ecological, Hydrological, and Atmospheric Studies: Technical Description and User's Guide.

Bonan, G.B., Patton, E.G., Harman, I.N., Oleson, K.W., Finnigan, J.J., Lu, Y., Burakowski, E.A., 2018. Modeling canopy-induced turbulence in the Earth system: a unified parameterization of turbulent exchange within plant canopies and the roughness sublayer (CLM-ml v0). Geoscientific Model Development 11, 1467–1496. https://doi.org/10.5194/gmd-11-1467-2018

Bonan, G.B., Williams, M., Fisher, R.A., Oleson, K.W., 2014. Modeling stomatal conductance in the earth system: linking leaf water-use efficiency and water transport along the soil–plant–atmosphere continuum. Geoscientific Model Development 7, 2193–2222. https://doi.org/10.5194/gmd-7-2193-2014

Bu, T., Wang, C., Chen, H., Meng, X., Li, Z., Chen, Y., Sheng, D., Zhao, C., 2024. An Investigation into the Applicability of the SHUD Model for Streamflow Simulation Based on CMFD Meteorological Data in the Yellow River Source Region. Water 16, 3583. https://doi.org/10.3390/w16243583

Cai, W., Yuan, W., Liang, S., Liu, S., Dong, W., Chen, Y., Liu, D., Zhang, H., 2014. Large Differences in Terrestrial Vegetation Production Derived from Satellite-Based Light Use Efficiency Models. Remote Sensing 6, 8945–8965. https://doi.org/10.3390/rs6098945

Cai, X., Yang, Z.-L., David, C.H., Niu, G.-Y., Rodell, M., 2014. Hydrological evaluation of the Noah-MP land surface model for the Mississippi River Basin. Journal of Geophysical Research: Atmospheres 119, 23–38. https://doi.org/10.1002/2013JD020792

Cai, X., Yang, Z.-L., Fisher, J.B., Zhang, X., Barlage, M., Chen, F., 2016. Integration of nitrogen dynamics into the Noah-MP land surface model v1.1 for climate and environmental predictions. Geoscientific Model Development 9, 1–15. https://doi.org/10.5194/gmd-9-1-2016

Chang, M., Liao, W., Wang, X., Zhang, Q., Chen, W., Wu, Z., Hu, Z., 2020. An optimal ensemble of the Noah-MP land surface model for simulating surface heat fluxes over a typical subtropical forest in South China. Agricultural and Forest Meteorology 281, 107815. https://doi.org/10.1016/j.agrformet.2019.107815

Chang, X., Xing, Y., Gong, W., Yang, C., Guo, Z., Wang, D., Wang, J., Yang, H., Xue, G., Yang, S., 2023. Evaluating gross primary productivity over 9 ChinaFlux sites based on random forest regression models, remote sensing, and eddy covariance data. Science of The Total Environment 875, 162601. https://doi.org/10.1016/j.scitotenv.2023.162601

Chen, F., Dudhia, J., 2001. Coupling an Advanced Land Surface–Hydrology Model with the Penn State–NCAR MM5 Modeling System. Part I: Model Implementation and Sensitivity. Monthly Weather Review 129, 569–585. https://doi.org/10.1175/1520-0493(2001)129%253C0569:CAALSH%253E2.0.CO;2

Chen, F., Janjić, Z., Mitchell, K., 1997. Impact of Atmospheric Surface-layer Parameterizations in the new Land-surface Scheme of the NCEP Mesoscale Eta Model. Boundary-Layer Meteorology 85, 391–421. https://doi.org/10.1023/A:1000531001463

Chen, J.M., Mo, G., Pisek, J., Liu, J., Deng, F., Ishizawa, M., Chan, D., 2012. Effects of foliage clumping on the estimation of global terrestrial gross primary productivity. Global Biogeochemical Cycles 26. https://doi.org/10.1029/2010GB003996

Chen, S.-P., Cui-Hai, Y.O.U., Zhong-Min, H.U., Zhi, C., Lei-Ming, Z., Qiu-Feng, W., 2020. Eddy covariance technique and its applications in flux observations of terrestrial ecosystems. Chinese Journal of Plant Ecology 44, 291. https://doi.org/10.17521/cjpe.2019.0351

Clark, M.P., Kavetski, D., Fenicia, F., 2011. Pursuing the method of multiple working hypotheses for hydrological modeling. Water Resources Research 47. https://doi.org/10.1029/2010WR009827

Clark, M.P., Nijssen, B., Lundquist, J.D., Kavetski, D., Rupp, D.E., Woods, R.A., Freer, J.E., Gutmann, E.D., Wood, A.W., Gochis, D.J., Rasmussen, R.M., Tarboton, D.G., Mahat, V., Flerchinger, G.N., Marks, D.G., 2015. A unified approach for process-based hydrologic modeling: 2. Model implementation and case studies. Water Resources Research 51, 2515–2542. https://doi.org/10.1002/2015WR017200

Clark, M.P., Schaefli, B., Schymanski, S.J., Samaniego, L., Luce, C.H., Jackson, B.M., Freer, J.E., Arnold, J.R., Moore, R.D., Istanbulluoglu, E., Ceola, S., 2016. Improving the theoretical underpinnings of process-based hydrologic models. Water Resources Research 52, 2350–2365. https://doi.org/10.1002/2015WR017910

Deardorff, J.W., 1977. A Parameterization of Ground-Surface Moisture Content for Use in Atmospheric Prediction Models.

Denning, A.S., Collatz, G.J., Zhang, C., Randall, D.A., Berry, J.A., Sellers, P.J., Colello, G.D., Dazlich, D.A., 1996. Simulations of terrestrial carbon metabolism and atmospheric CO_2 in a general circulation model: Part 1:

https://doi.org/10.5194/egusphere-2026-103
Preprint. Discussion started: 29 January 2026

Surface carbon fluxes. Tellus B: Chemical and Physical Meteorology 48, 521. https://doi.org/10.3402/tellusb.v48i4.15930

Dickinson, R.E., 1983. Land Surface Processes and Climate—Surface Albedos and Energy Balance, in: Saltzman, B. (Ed.), Advances in Geophysics, Theory of Climate. Elsevier, pp. 305–353. https://doi.org/10.1016/S0065-2687(08)60176-4

Dickinson, R.E., Shaikh, M., Bryant, R., Graumlich, L., 1998. Interactive Canopies for a Climate Model.

Dyer, A.J., 1974. A review of flux-profile relationships. Boundary-Layer Meteorol 7, 363–372. https://doi.org/10.1007/BF00240838

Ensminger, I., Busch, F., Huner, N.P.A., 2006. Photostasis and cold acclimation: sensing low temperature through photosynthesis.

Finnigan, J., 2000. Turbulence in Plant Canopies. Annual Review of Fluid Mechanics 32, 519–571. https://doi.org/10.1146/annurev.fluid.32.1.519

Fu, Z., Stoy, P.C., Luo, Y., Chen, J., Sun, J., Montagnani, L., Wohlfahrt, G., Rahman, A.F., Rambal, S., Bernhofer, C., Wang, J., Shirkey, G., Niu, S., 2017. Climate controls over the net carbon uptake period and amplitude of net ecosystem production in temperate and boreal ecosystems. Agricultural and Forest Meteorology 243, 9–18. https://doi.org/10.1016/j.agrformet.2017.05.009

Gan, Y., Liang, X.-Z., Duan, Q., Chen, F., Li, J., Zhang, Y., 2019. Assessment and Reduction of the Physical Parameterization Uncertainty for Noah-MP Land Surface Model. Water Resources Research 55, 5518–5538. https://doi.org/10.1029/2019WR024814

Gim, H.-J., Park, S.K., Kang, M., Thakuri, B.M., Kim, J., Ho, C.-H., 2017. An improved parameterization of the allocation of assimilated carbon to plant parts in vegetation dynamics for Noah-MP. Journal of Advances in Modeling Earth Systems 9, 1776–1794. https://doi.org/10.1002/2016MS000890

Green, J.K., Konings, A.G., Alemohammad, S.H., Berry, J., Entekhabi, D., Kolassa, J., Lee, J.-E., Gentine, P., 2017. Regionally strong feedbacks between the atmosphere and terrestrial biosphere. Nature Geosci 10, 410–414. https://doi.org/10.1038/ngeo2957

He, C., Chen, F., Barlage, M., Yang, Z.-L., Wegiel, J.W., Niu, G.-Y., Gochis, D., Mocko, D.M., Abolafia-Rosenzweig, R., Zhang, Z., Lin, T.-S., Valayamkunnath, P., Ek, M., Niyogi, D., 2023. Enhancing the Community Noah-MP Land Model Capabilities for Earth Sciences and Applications. Bulletin of the American Meteorological Society 104, E2023–E2029. https://doi.org/10.1175/BAMS-D-23-0249.1

He, J., Yang, K., Li, X., Tang, W., SHAO Changkun,JIANG Yaozhi,DING Baohong, 2025. China meteorological forcing dataset v2.0 (1951-2020). National Tibetan Plateau Data Center. https://doi.org/10.11888/Atmos.tpdc.302088

He, S., Zhang, Y., Ma, N., Tian, J., Kong, D., Liu, C., 2022. A daily and 500m coupled evapotranspiration and gross primary production product across China during 2000–2020. Earth System Science Data 14, 5463–5488. https://doi.org/10.5194/essd-14-5463-2022

He, X., Liu, S., Bateni, S.M., Xu, T., Jun, C., Kim, D., Li, X., Song, L., Zhao, L., Xu, Z., Wei, J., 2024. Innovative approach for estimating evapotranspiration and gross primary productivity by integrating land data assimilation, machine learning, and multi-source observations. Agricultural and Forest Meteorology 355, 110136. https://doi.org/10.1016/j.agrformet.2024.110136

Huang, L., Liu, M., Yao, N., 2023. Evaluation of Ecosystem Water Use Efficiency Based on Coupled and Uncoupled Remote Sensing Products for Maize and Soybean. Remote Sensing 15, 4922. https://doi.org/10.3390/rs15204922

Immerzeel, W.W., van Beek, L.P.H., Bierkens, M.F.P., 2010. Climate Change Will Affect the Asian Water Towers. Science 328, 1382–1385. https://doi.org/10.1126/science.1183188

Jasechko, S., Sharp, Z.D., Gibson, J.J., Birks, S.J., Yi, Y., Fawcett, P.J., 2013. Terrestrial water fluxes dominated by transpiration. Nature 496, 347–350. https://doi.org/10.1038/nature11983

Kannenberg, S.A., Anderegg, W.R.L., Barnes, M.L., Dannenberg, M.P., Knapp, A.K., 2024. Dominant role of soil moisture in mediating carbon and water fluxes in dryland ecosystems. Nat. Geosci. 17, 38–43. https://doi.org/10.1038/s41561-023-01351-8

Keys to Soil Taxonomy, 13th Edition, n.d.

Knapp, A.K., Beier, C., Briske, D.D., Classen, A.T., Luo, Y., Reichstein, M., Smith, M.D., Smith, S.D., Bell, J.E., Fay, P.A., Heisler, J.L., Leavitt, S.W., Sherry, R., Smith, B., Weng, E., 2008. Consequences of More Extreme Precipitation Regimes for Terrestrial Ecosystems. BioScience 58, 811–821. https://doi.org/10.1641/B580908

lai, jie, 2026. Code and Data. https://doi.org/10.5281/zenodo.18158937

https://doi.org/10.5194/egusphere-2026-103
Preprint. Discussion started: 29 January 2026

Lei, H., Huang, M., Leung, L.R., Yang, D., Shi, X., Mao, J., Hayes, D.J., Schwalm, C.R., Wei, Y., Liu, S., 2014. Sensitivity of global terrestrial gross primary production to hydrologic states simulated by the Community Land Model using two runoff parameterizations. Journal of Advances in Modeling Earth Systems 6, 658–679. https://doi.org/10.1002/2013MS000252

Li, J., Miao, C., Zhang, G., Fang, Y.-H., Shangguan, W., Niu, G.-Y., 2022. Global Evaluation of the Noah-MP Land Surface Model and Suggestions for Selecting Parameterization Schemes. Journal of Geophysical Research: Atmospheres 127, e2021JD035753. https://doi.org/10.1029/2021JD035753

Li, L., Yang, Z.-L., Matheny, A.M., Zheng, H., Swenson, S.C., Lawrence, D.M., Barlage, M., Yan, B., McDowell, N.G., Leung, L.R., 2021. Representation of Plant Hydraulics in the Noah-MP Land Surface Model: Model Development and Multiscale Evaluation. Journal of Advances in Modeling Earth Systems 13, e2020MS002214. https://doi.org/10.1029/2020MS002214

Li, W.-P., Zhang, Y.-W., Mu, M., Shi, X.-L., Zhou, W.-Y., Ji, J.-J., 2023. Spatial and temporal variations of gross primary production simulated by land surface model BCC_AVIM2.0. Advances in Climate Change Research, Special Issue on Changing Boreal-Arctic Permafrost and Snow-cover and Their Impacts 14, 286–299. https://doi.org/10.1016/j.accre.2023.02.001

Li, X., Hu, Z.-Z., Liang, P., Zhu, J., 2019. Contrastive Influence of ENSO and PNA on Variability and Predictability of North American Winter Precipitation. https://doi.org/10.1175/JCLI-D-19-0033.1

Ma, N., Niu, G.-Y., Xia, Y., Cai, X., Zhang, Y., Ma, Y., Fang, Y., 2017. A Systematic Evaluation of Noah-MP in Simulating Land-Atmosphere Energy, Water, and Carbon Exchanges Over the Continental United States. Journal of Geophysical Research: Atmospheres 122, 12,245-12,268. https://doi.org/10.1002/2017JD027597

Manabe, S., 1969. CLIMATE AND THE OCEAN CIRCULATION.

Misson, L., Baldocchi, D.D., Black, T.A., Blanken, P.D., Brunet, Y., Curiel Yuste, J., Dorsey, J.R., Falk, M., Granier, A., Irvine, M.R., Jarosz, N., Lamaud, E., Launiainen, S., Law, B.E., Longdoz, B., Loustau, D., McKay, M., Paw U, K.T., Vesala, T., Vickers, D., Wilson, K.B., Goldstein, A.H., 2007. Partitioning forest carbon fluxes with overstory and understory eddy-covariance measurements: A synthesis based on FLUXNET data. Agricultural and Forest Meteorology 144, 14–31. https://doi.org/10.1016/j.agrformet.2007.01.006

Nelson, J.A., Carvalhais, N., Migliavacca, M., Reichstein, M., Jung, M., 2018. Water-stress-induced breakdown of carbon–water relations: indicators from diurnal FLUXNET patterns. Biogeosciences 15, 2433–2447. https://doi.org/10.5194/bg-15-2433-2018

Niu, G.-Y., Yang, Z.-L., 2007. An observation-based formulation of snow cover fraction and its evaluation over large North American river basins. Journal of Geophysical Research: Atmospheres 112. https://doi.org/10.1029/2007JD008674

Niu, G.-Y., Yang, Z.-L., 2004. Effects of vegetation canopy processes on snow surface energy and mass balances. Journal of Geophysical Research: Atmospheres 109. https://doi.org/10.1029/2004JD004884

Niu, G.-Y., Yang, Z.-L., Dickinson, R.E., Gulden, L.E., 2005. A simple TOPMODEL-based runoff parameterization (SIMTOP) for use in global climate models. Journal of Geophysical Research: Atmospheres 110. https://doi.org/10.1029/2005JD006111

Niu, G.-Y., Yang, Z.-L., Mitchell, K.E., Chen, F., Ek, M.B., Barlage, M., Kumar, A., Manning, K., Niyogi, D., Rosero, E., Tewari, M., Xia, Y., 2011. The community Noah land surface model with multiparameterization options (Noah-MP): 1. Model description and evaluation with local-scale measurements. Journal of Geophysical Research: Atmospheres 116. https://doi.org/10.1029/2010JD015139

Oleson, A.K., Lawrence, A.D., Bonan, A.G., Flanner, A.M., Kluzek, A.E., Lawrence, A.P., Levis, A.S., Swenson, A.S., Thornton, A.P., Dai, A.A., Decker, A.M., Dickinson, A.R., Feddema, A.J., Heald, A.C., Hoffman, A.F., Lamarque, A.J., Mahowald, A.N., Niu, A.G., Qian, A.T., Randerson, A.J., Running, A.S., Sakaguchi, A.K., Slater, A.A., Stockli, A.R., Wang, A.A., Yang, A.Z., Zeng, A.X., Division (CGD), C.U.C.F.A.R. (UCAR):National C. for A.R. (NCAR):NCAR E.S.L. (NESL):Climate and G.D., 2010. Technical Description of version 4.0 of the Community Land Model (CLM). University Corporation for Atmospheric Research. https://doi.org/10.5065/D6FB50WZ

Piao, S., Sitch, S., Ciais, P., Friedlingstein, P., Peylin, P., Wang, X., Ahlström, A., Anav, A., Canadell, J., Cong, N., Huntingford, C., Jung, M., Levis, S., Levy, P.E., Li, J., Lin, X., Lomas, M., Lu, M., Luo, Y., Ma, Y., Myneni, R., Poulter, B., Sun, Z., Wang, T., Viovy, N., Zaehle, S., Zeng, N., 2013. Evaluation of terrestrial carbon cycle models for their response to climate variability and to CO_2 trends. Global Change Biology 19, 2117–2132. https://doi.org/10.1111/gcb.12187

Pitman, A.J., 2003. The evolution of, and revolution in, land surface schemes designed for climate models. Intl Journal of Climatology 23, 479–510. https://doi.org/10.1002/joc.893

https://doi.org/10.5194/egusphere-2026-103
Preprint. Discussion started: 29 January 2026

Poggio, L., de Sousa, L.M., Batjes, N.H., Heuvelink, G.B.M., Kempen, B., Ribeiro, E., Rossiter, D., 2021. SoilGrids 2.0: producing soil information for the globe with quantified spatial uncertainty. SOIL 7, 217–240. https://doi.org/10.5194/soil-7-217-2021

Qian, L., Yu, X., Zhang, Z., Wu, L., Fan, J., Xiang, Y., Chen, J., Liu, X., 2024. Assessing and improving the high uncertainty of global gross primary productivity products based on deep learning under extreme climatic conditions. Science of The Total Environment 957, 177344. https://doi.org/10.1016/j.scitotenv.2024.177344

Qiu, R., Han, G., Ma, X., Xu, H., Shi, T., Zhang, M., 2020. A Comparison of OCO-2 SIF, MODIS GPP, and GOSIF Data from Gross Primary Production (GPP) Estimation and Seasonal Cycles in North America. Remote Sensing 12, 258. https://doi.org/10.3390/rs12020258

Reich, P.B., Walters, M.B., Ellsworth, D.S., 1997. From tropics to tundra: Global convergence in plant functioning. Proceedings of the National Academy of Sciences 94, 13730–13734. https://doi.org/10.1073/pnas.94.25.13730

Running, S.W., Nemani, R.R., Heinsch, F.A., Zhao, M., Reeves, M., Hashimoto, H., 2004. A Continuous Satellite-Derived Measure of Global Terrestrial Primary Production. BioScience 54, 547–560. https://doi.org/10.1641/0006-3568(2004)054%255B0547:ACSMOG%255D2.0.CO;2

Saltelli, A., Annoni, P., Azzini, I., Campolongo, F., Ratto, M., Tarantola, S., 2010. Variance based sensitivity analysis of model output. Design and estimator for the total sensitivity index. Computer Physics Communications 181, 259–270. https://doi.org/10.1016/j.cpc.2009.09.018

Saltelli, A., Sobol, I.M., 1995. Sensitivity Analysis for Nonlinear Mathematical Models. Numerical Experience Sensitivity Analysis for Nonlinear Mathematical Models. Numerical Experience. Matematicheskoe Modelirovanie.

Schaake, J.C., Koren, V.I., Duan, Q.-Y., Mitchell, K., Chen, F., 1996. Simple water balance model for estimating runoff at different spatial and temporal scales. Journal of Geophysical Research: Atmospheres 101, 7461–7475. https://doi.org/10.1029/95JD02892

Schaefer, K., Schwalm, C.R., Williams, C., Arain, M.A., Barr, A., Chen, J.M., Davis, K.J., Dimitrov, D., Hilton, T.W., Hollinger, D.Y., Humphreys, E., Poulter, B., Raczka, B.M., Richardson, A.D., Sahoo, A., Thornton, P., Vargas, R., Verbeeck, H., Anderson, R., Baker, I., Black, T.A., Bolstad, P., Chen, J., Curtis, P.S., Desai, A.R., Dietze, M., Dragoni, D., Gough, C., Grant, R.F., Gu, L., Jain, A., Kucharik, C., Law, B., Liu, S., Lokipitiya, E., Margolis, H.A., Matamala, R., McCaughey, J.H., Monson, R., Munger, J.W., Oechel, W., Peng, C., Price, D.T., Ricciuto, D., Riley, W.J., Roulet, N., Tian, H., Tonitto, C., Torn, M., Weng, E., Zhou, X., 2012. A model-data comparison of gross primary productivity: Results from the North American Carbon Program site synthesis. Journal of Geophysical Research: Biogeosciences 117. https://doi.org/10.1029/2012JG001960

Schlesinger, W.H., Reynolds, J.F., Cunningham, G.L., Huenneke, L.F., Jarrell, W.M., Virginia, R.A., Whitford, W.G., 1990. Biological Feedbacks in Global Desertification. Science 247, 1043–1048. https://doi.org/10.1126/science.247.4946.1043

Schwinning, S., Sala, O.E., 2004. Hierarchy of responses to resource pulses in arid and semi-arid ecosystems. Oecologia 141, 211–220. https://doi.org/10.1007/s00442-004-1520-8

SELLERS, P.J., 1985. Canopy reflectance, photosynthesis and transpiration. International Journal of Remote Sensing 6, 1335–1372. https://doi.org/10.1080/01431168508948283

Sellers, P.J., Dickinson, R.E., Randall, D.A., Betts, A.K., Hall, F.G., Berry, J.A., Collatz, G.J., Denning, A.S., Mooney, H.A., Nobre, C.A., Sato, N., Field, C.B., Henderson-Sellers, A., 1997. Modeling the Exchanges of Energy, Water, and Carbon Between Continents and the Atmosphere. Science 275, 502–509. https://doi.org/10.1126/science.275.5299.502

Shi, X., She, D., Xia, J., Liu, R., Wang, T., 2024. The intercomparison of six 0.1°×0.1° spatial resolution evapotranspiration products across mainland China. Journal of Hydrology 633, 130949. https://doi.org/10.1016/j.jhydrol.2024.130949

Sims, D.A., Rahman, A.F., Cordova, V.D., El-Masri, B.Z., Baldocchi, D.D., Bolstad, P.V., Flanagan, L.B., Goldstein, A.H., Hollinger, D.Y., Misson, L., Monson, R.K., Oechel, W.C., Schmid, H.P., Wofsy, S.C., Xu, L., 2008. A new model of gross primary productivity for North American ecosystems based solely on the enhanced vegetation index and land surface temperature from MODIS. Remote Sensing of Environment, Remote Sensing Data Assimilation Special Issue 112, 1633–1646. https://doi.org/10.1016/j.rse.2007.08.004

Sobol′, I.M., 2001. Global sensitivity indices for nonlinear mathematical models and their Monte Carlo estimates. Mathematics and Computers in Simulation 55, 271–280. https://doi.org/10.1016/S0378-4754(00)00270-6

https://doi.org/10.5194/egusphere-2026-103
Preprint. Discussion started: 29 January 2026

Stöckli, R., Lawrence, D.M., Niu, G.-Y., Oleson, K.W., Thornton, P.E., Yang, Z.-L., Bonan, G.B., Denning, A.S., Running, S.W., 2008. Use of FLUXNET in the Community Land Model development. Journal of Geophysical Research: Biogeosciences 113. https://doi.org/10.1029/2007JG000562

Stoy, P.C., Katul, G.G., Siqueira, M.B.S., Juang, J.-Y., Novick, K.A., Uebelherr, J.M., Oren, R., 2006. An evaluation of models for partitioning eddy covariance-measured net ecosystem exchange into photosynthesis and respiration. Agricultural and Forest Meteorology 141, 2–18. https://doi.org/10.1016/j.agrformet.2006.09.001

Sulla-Menashe, D., Friedl, M.A., 2022. User Guide to Collection 6 MODIS Land Cover (MCD12Q1 and MCD12C1) Product.

Taylor, K.E., 2001. Summarizing multiple aspects of model performance in a single diagram. Journal of Geophysical Research: Atmospheres 106, 7183–7192. https://doi.org/10.1029/2000JD900719

Vicca, S., 2018. Global vegetation's CO2 uptake. Nat Ecol Evol 2, 1840–1841. https://doi.org/10.1038/s41559-018-0730-0

Wang, B., Zhu, G.-F., Zhong, J.-T., Ma, C.-F., Zhang, L., Tan, M.-B., Li, X., 2025. Uncertainty analysis and parameter optimization of a water yield ecosystem service model: A case study of the Qilian Mountains, China. Science of The Total Environment 966, 178772. https://doi.org/10.1016/j.scitotenv.2025.178772

Wang, F., Li, Y., Li, Z., Cai, X., Lin, X., Guo, L., Han, D., Fang, J., 2024. Enhancing Winter Wheat Representation in Noah-MP-Crop for Improved Dynamic Crop Growth Simulation in the North China Plain. Journal of Geophysical Research: Biogeosciences 129, e2024JG008150. https://doi.org/10.1029/2024JG008150

Wang, H., Shao, W., Hu, Y., Cao, W., Zhang, Y., 2023. Assessment of Six Machine Learning Methods for Predicting Gross Primary Productivity in Grassland. Remote Sensing 15, 3475. https://doi.org/10.3390/rs15143475

Wang, L., Yu, M., Ye, S., Yan, J., 2023. Seasonal patterns of carbon and water flux responses to precipitation and solar radiation variability in a subtropical evergreen forest, South China. Agricultural and Forest Meteorology 342, 109760. https://doi.org/10.1016/j.agrformet.2023.109760

Wang, S., Fu, B., Wei, F., Piao, S., Maestre, F.T., Wang, L., Jiao, W., Liu, Y., Li, Y., Li, C., Zhao, W., 2023. Drylands contribute disproportionately to observed global productivity increases. Science Bulletin 68, 224–232. https://doi.org/10.1016/j.scib.2023.01.014

Wang, Y., Xu, X., Liu, H., Li, Yueqing, Li, Yaohui, Hu, Z., Gao, X., Ma, Y., Sun, J., Lenschow, D.H., Zhong, S., Zhou, M., Bian, X., Zhao, P., 2016. Analysis of land surface parameters and turbulence characteristics over the Tibetan Plateau and surrounding region. Journal of Geophysical Research: Atmospheres 121, 9540–9560. https://doi.org/10.1002/2016JD025401

Wang, Yunlong, Zhou, G., Wang, Yuhui, 2008. Environmental effects on net ecosystem CO2 exchange at half-hour and month scales over *Stipa krylovii* steppe in northern China. Agricultural and Forest Meteorology, AsiaFlux Special Issue 148, 714–722. https://doi.org/10.1016/j.agrformet.2008.01.013

Waring, R.H., Landsberg, J.J., Williams, M., 1998. Net primary production of forests: a constant fraction of gross primary production? Tree Physiology 18, 129–134. https://doi.org/10.1093/treephys/18.2.129

Wei, S., Yi, C., Fang, W., Hendrey, G., 2017. A global study of GPP focusing on light-use efficiency in a random forest regression model. Ecosphere 8, e01724. https://doi.org/10.1002/ecs2.1724

Winkler, D.E., Butz, R.J., Germino, M.J., Reinhardt, K., Kueppers, L.M., 2018. Snowmelt Timing Regulates Community Composition, Phenology, and Physiological Performance of Alpine Plants. Front. Plant Sci. 9. https://doi.org/10.3389/fpls.2018.01140

Wolf, S., Keenan, T.F., Fisher, J.B., Baldocchi, D.D., Desai, A.R., Richardson, A.D., Scott, R.L., Law, B.E., Litvak, M.E., Brunsell, N.A., Peters, W., van der Laan-Luijkx, I.T., 2016. Warm spring reduced carbon cycle impact of the 2012 US summer drought. Proceedings of the National Academy of Sciences 113, 5880–5885. https://doi.org/10.1073/pnas.1519620113

Xue, Y., Sellers, P.J., Kinter, J.L., Shukla, J., 1991. A Simplified Biosphere Model for Global Climate Studies. Journal of Climate 4, 345–364. https://doi.org/10.1175/1520-0442(1991)004%253C0345:ASBMFG%253E2.0.CO;2

Yang, Q., Dan, L., Lv, M., Wu, J., Li, W., Dong, W., 2021. Quantitative assessment of the parameterization sensitivity of the Noah-MP land surface model with dynamic vegetation using ChinaFLUX data. Agricultural and Forest Meteorology 307, 108542. https://doi.org/10.1016/j.agrformet.2021.108542

Yang, R., Friedl, M.A., 2003. Modeling the effects of three-dimensional vegetation structure on surface radiation and energy balance in boreal forests. Journal of Geophysical Research: Atmospheres 108. https://doi.org/10.1029/2002JD003109

https://doi.org/10.5194/egusphere-2026-103
Preprint. Discussion started: 29 January 2026

Yang, X., Yong, B., Ren, L., Zhang, Y., Long, D., 2017. Multi-scale validation of GLEAM evapotranspiration products over China via ChinaFLUX ET measurements. International Journal of Remote Sensing.

Yang, Z.-L., Dickinson, R.E., 1996. Description of the Biosphere-Atmosphere Transfer Scheme (BATS) for the Soil Moisture Workshop and evaluation of its performance. Global and Planetary Change, Soil Moisture Simulation 13, 117–134. https://doi.org/10.1016/0921-8181(95)00041-0

Yang, Z.-L., Niu, G.-Y., 2003. The Versatile Integrator of Surface and Atmosphere processes: Part 1. Model description. Global and Planetary Change, Project for Intercomparison of Land-surface Parameterization Schemes, Phase 2(e) 38, 175–189. https://doi.org/10.1016/S0921-8181(03)00028-6

Yang, Z.-L., Niu, G.-Y., Mitchell, K.E., Chen, F., Ek, M.B., Barlage, M., Longuevergne, L., Manning, K., Niyogi, D., Tewari, M., Xia, Y., 2011. The community Noah land surface model with multiparameterization options (Noah-MP): 2. Evaluation over global river basins. Journal of Geophysical Research: Atmospheres 116. https://doi.org/10.1029/2010JD015140

You, Y., Huang, C., Yang, Z., Zhang, Y., Bai, Y., Gu, J., 2020. Assessing Noah-MP Parameterization Sensitivity and Uncertainty Interval Across Snow Climates. Journal of Geophysical Research: Atmospheres 125, e2019JD030417. https://doi.org/10.1029/2019JD030417

You, Y., Huang, C., Zhang, Y., 2024. Assessing the Sensitivity of Snow Depth Simulations to Land Surface Parameterizations within Noah-MP in Northern Xinjiang, China. Remote Sensing 16, 594. https://doi.org/10.3390/rs16030594

Yu, G., Ren, W., Chen, Z., Zhang, Leiming, Wang, Q., Wen, X., He, N., Zhang, Li, Fang, H., Zhu, X., Gao, Y., Sun, X., 2016. Construction and progress of Chinese terrestrial ecosystem carbon, nitrogen and water fluxes coordinated observation. J. Geogr. Sci. 26, 803–826. https://doi.org/10.1007/s11442-016-1300-5

Yuan, W., Liu, S., Zhou, Guangsheng, Zhou, Guoyi, Tieszen, L.L., Baldocchi, D., Bernhofer, C., Gholz, H., Goldstein, A.H., Goulden, M.L., Hollinger, D.Y., Hu, Y., Law, B.E., Stoy, P.C., Vesala, T., Wofsy, S.C., 2007. Deriving a light use efficiency model from eddy covariance flux data for predicting daily gross primary production across biomes. Agricultural and Forest Meteorology 143, 189–207. https://doi.org/10.1016/j.agrformet.2006.12.001

Zhang, L., Mao, J., Shi, X., Ricciuto, D., He, H., Thornton, P., Yu, G., Li, P., Liu, M., Ren, X., Han, S., Li, Y., Yan, J., Hao, Y., Wang, H., 2016. Evaluation of the Community Land Model simulated carbon and water fluxes against observations over ChinaFLUX sites. Agricultural and Forest Meteorology 226–227, 174–185. https://doi.org/10.1016/j.agrformet.2016.05.018

Zhang, R., Chen, S., 2025. Spatiotemporal analysis, simulation, and early warning of landslides based on landslide sensitivity and multisource precipitation products in Southwestern China. Landslides. https://doi.org/10.1007/s10346-024-02437-z

Zhang, Y., Ye, A., 2022. Uncertainty analysis of multiple terrestrial gross primary productivity products. Global Ecol Biogeogr 31, 2204–2218. https://doi.org/10.1111/geb.13578

Zheng, H., Yang, Z.-L., Lin, P., Wei, J., Wu, W.-Y., Li, L., Zhao, L., Wang, S., 2019. On the Sensitivity of the Precipitation Partitioning Into Evapotranspiration and Runoff in Land Surface Parameterizations. Water Resources Research 55, 95–111. https://doi.org/10.1029/2017WR022236

Zheng, Y., Zhang, L., Li, P., Ren, X., He, H., Lv, Y., Ma, Y., 2023. Evaluation of the Community Land Model-Simulated Specific Leaf Area with Observations over China: Impacts on Modeled Gross Primary Productivity. Forests 14, 164. https://doi.org/10.3390/f14010164

Zhou, S., Zhang, Y., Park Williams, A., Gentine, P., 2019. Projected increases in intensity, frequency, and terrestrial carbon costs of compound drought and aridity events. Science Advances 5, eaau5740. https://doi.org/10.1126/sciadv.aau5740